LA-UR-16-27510
Approved for public release; distribution is unlimited.

Title: Nightshade Prototype Experiments (Silverleaf)

Author(s): Danielson, Jeremy
Bauer, Amy L.

Intended for: Report

Issued: 2016-12-23 (rev.1)

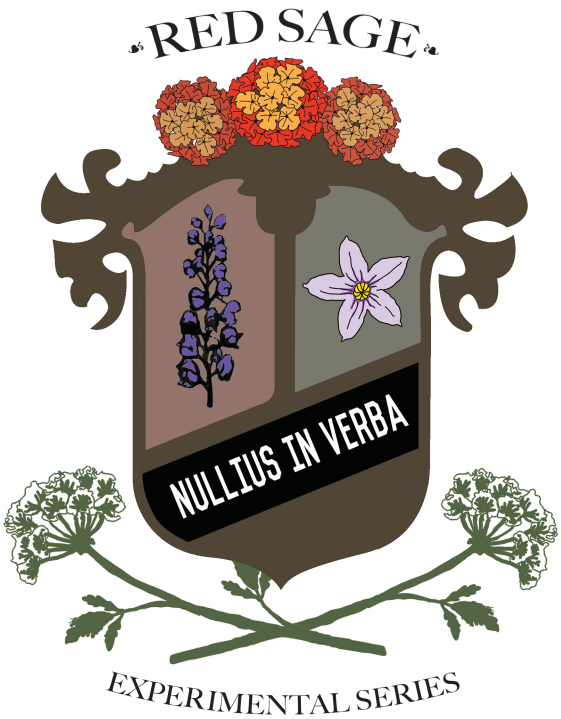

Nightshade Prototype Experiments (Silverleaf)

Jeremy Danielson, Physics Division

Amy Bauer, X Theoretical Design Division

Los Alamos National Laboratory (LANL)

September 2016

LA-UR-16-27510

Table of Contents

Executive Summary

The Red Sage campaign is a series of subcritical dynamic plutonium experiments designed to measure ejecta. Nightshade, the first experiments in Red Sage scheduled for fiscal year 2019, will measure the amount of ejecta emission into vacuum from a double-shocked plutonium surface. To address the major technical risks in Nightshade, a Level 2 milestone was developed for fiscal year 2016. The milestone reads:

> "Validate the preliminary Nightshade in-vessel fielding geometry by demonstrating inter-diagnostic agreement with the relevant geometries, stand-off distances, and conjugates."

Silverleaf, a series of four experiments, was executed at the Los Alamos National Laboratory in July and August 2016 to demonstrate a prototype of the Nightshade package and to satisfy this Level 2 milestone. This report is documentation that Red Sage Level 2 milestone requirements were successfully met.

The Silverleaf package was a good initial design, and succeeded in meeting the constraints for fielding at the Nevada National Security Site U1a facility. All the diagnostics functioned well and excellent data was obtained, one of the major technical concerns for the Nightshade series due to the complexity of the experimental design. The assembly quality and the data quality improved with each experiment.

The Silverleaf PDV measurements showed many interesting features, including multiple surfaces and significant ejecta. Data analysis shows excellent consistency among the various diagnostics, even with variation stemming from the inhomogeneity of the ejecta cloud. The independent ejecta diagnostics quantitatively agreed well with each other. In addition, PDV and high-speed camera data showed no evidence of package interference. A 1 μs margin was measured between the shock transit time through the hex housing to the diagnostic feedthroughs and the end of the experiment, indicating a good hex housing design and assembly. Broadband laser ranging was successfully fielded for the first time, which lays the groundwork for fielding this diagnostic on the Eurydice subcritical experiment.

As a result of the Silverleaf series, a number of design improvements have been identified for the Nightshade experiments. These improvements cover many aspects of the design, from diagnostic improvements to manufacturing and assembly methods that will result in a more efficient and higher quality experiment.

The Red Sage team has demonstrated significant progress and a path forward for the successful execution of Nightshade in FY2019.

Introduction

The Red Sage campaign is a series of subcritical dynamic plutonium experiments designed to measure ejecta. Nightshade, the first of three experimental series (Wolfsbane and Hemlock are the subsequent two series), will measure the amount of ejecta emission into vacuum from a double-shocked plutonium surface. The Nightshade series will provide meaningful constraints on the source term in physics-based ejecta models. Currently Nightshade is scheduled to be executed at the Nevada National Security Site U1a facility in fiscal year 2019.

To prepare for the U1a experiments, an experimental series called Silverleaf was executed at the Los Alamos National Laboratory in July and August 2016 to exercise a prototype of the Nightshade package. These experiments were designed to fit the constraints of an experiment as it would be fielded at the U1a facility. The goal of these experiments was to address a major technical risk to the Nightshade series: several explosive packages need to fire at precise times to allow a number of different concurrent measurements. There was concern that the various explosive packages and diagnostics could interfere with each other.

Statement of Milestone

To address these concerns, a milestone was set for the fiscal year 2016.

"Milestone: Validate the preliminary Nightshade in-vessel fielding geometry by demonstrating inter-diagnostic agreement with the relevant geometries, stand-off distances, and conjugates."

The milestone deliverable is this report, which disseminates the work carried out this year to satisfy the milestone, specifically the Silverleaf series of experiments, and shows the comparison of radiographic and momentum-transfer ejecta mass-velocity diagnostics on double-shock ejecta packages in geometries representative of the Nightshade in-vessel design.

Nightshade Design Summary

The Nightshade double-shock drive package consists of a plane-wave high-explosive (HE) lens, a tantalum anvil, and a target. The purpose of the anvil is to provide a second shock to the target surface. A thin membrane in front of the target is necessary as an environmental seal, to avoid having the plutonium in direct physical contact with the explosive.

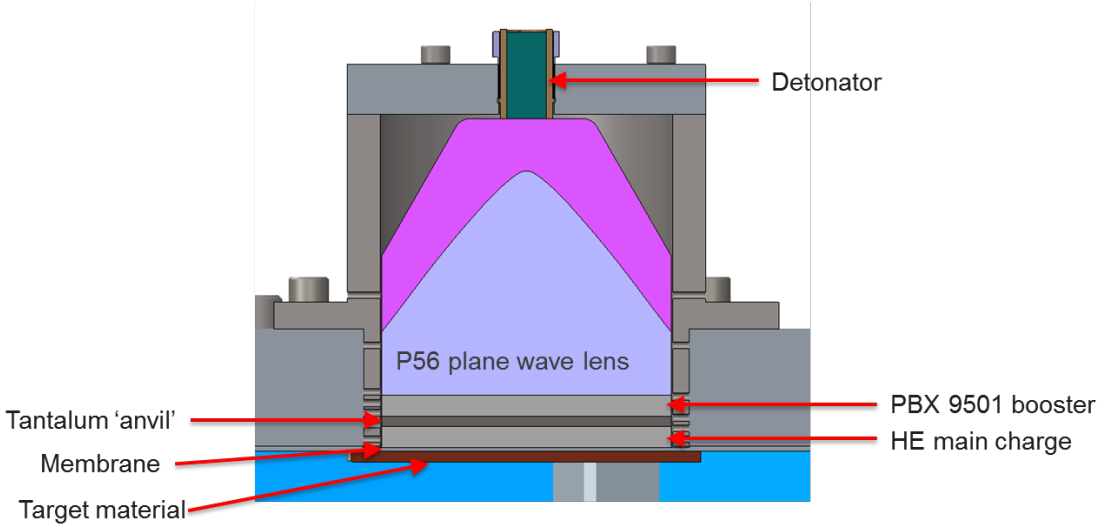

Figure 1: Nominal drive configuration for Nightshade double shock experiments.

On Nightshade, we will make precision measurements in a complicated environment. The amount of ejecta emitted upon second shock is very sensitive to the surface roughness of the target as well as the shock loading. The physics of spall and recollection cause inhomogeneity in the emission, and it is possible for ejecta emitted from the first shock to interfere with ejecta emitted from the second. For these reasons, Nightshade will be fielded with a large number of complementary diagnostics to more fully characterize the ejecta field. These diagnostics include:

- Momentum diagnostics:
- Lithium niobate ($LiNbO_3$) pins
- Asay foils
- Mass-density diagnostics:
- Multiple frame soft X-ray radiography
- Single frame Cygnus radiography
- Drive Package Diagnostics:
- Photonic Doppler velocimetry (PDV)
- Broadband laser ranging (BLR)
- Time of arrival diagnostic (TOAD)

By fielding a wide array of diagnostics with different systematic sensitivities and failure modes, a more comprehensive measurement of complex ejecta emission with tighter uncertainties can be obtained.

The Silverleaf Experiments

The Silverleaf experiments were designed to conform to a number of constraints on the future dynamic plutonium experiment, Nightshade. These constraints are:

- The experiment will be performed in a 3-foot vessel with radiographic ports set 60 degrees apart. To accommodate this, the package walls will be hexagonal for radiographic access. This package is referred to as a 'hex box' or 'hex housing'.
- The experiment will be fired under vacuum, so the samples and various probes will be mounted inside an evacuated hex box. The explosive charges will attach to the outside of this box (see figure 4).
- The hex box will be assembled with the target and populated with diagnostics at TA-55 in Los Alamos, without the explosive charges attached. The hex box containing samples and probes will be shipped to the Device Assembly Facility (DAF) separated from the explosive charges. The charges will be mounted at the DAF and then the complete package inserted at U1a.
- Each hex box will contain four explosive packages. The four explosive drives must not interfere with each other. Similarly, the various diagnostics must also not interfere with each other.
- To maximize the number of targets in the radiographic field of view, two explosive packages should fire upwards and two downwards. The diagnostics must be able to be oriented in either vertical direction.
- The feedthroughs bringing data channels through the hex box walls must retain vacuum and survive until after the experiment has finished.
- The soft x-rays will have to generate multiple images, and be transmitted through some amount of mitigation and window material.
- Each explosive drive must be detonated at different times (on the order of a few microseconds). This requires an independently timed fireset for each detonator.

For Silverleaf, it was decided that three drives and targets per experiment would be sufficient to exercise the hex box and diagnostic assembly design and to diagnose inter-package interference. Tin targets were used since there is a large body of work on ejecta production from shock-loaded tin. A total of four experiments – Silverleaf A through D - were fired in July and August 2016. Both the assembly quality and the data quality improved with each experiment. Silverleaf A showed strong artifacts in the data that appear to result from unrelieved stresses from the manufacturing methods used to fabricate the lid. These methods were changed for Silverleaf B-D, and those artifacts have been removed. Similarly, the vacuum seals, especially those for

the gas-blocked feedthroughs, were improved with each experiment. Silverleaf C and D attained the lowest vacuum and returned the best data quality.

Silverleaf Design[1]

Physics Requirements

Physics requirements for Red Sage/Nightshade were outlined in an XTD design release and can be summarized by the figure and table below. Figure 2 is the nominal experimental drive package configuration for the Nightshade series of experiments. Table 1 is the matrix of specific experimental drive configurations and target surface finishes fielded during the Silverleaf series. Silverleaf consisted of four experiments with three HE drives in each of the hex box assemblies. The various drive configurations were chosen to bound the extrema of ejecta production to be measured and to challenge the fireset timing in preparation for the confirmatory experiment Iris and the Nightshade series.

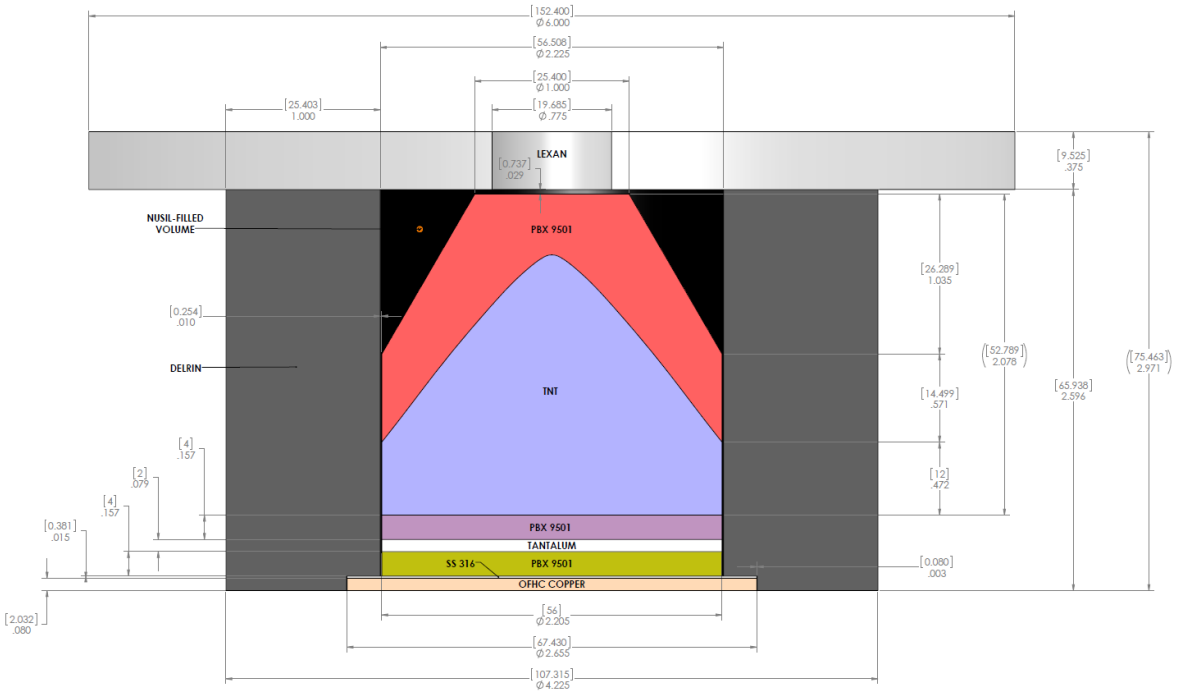

Figure 2: The nominal experimental drive package configuration.

[1] This section was contributed by Robert Gonzales (Q-18: Technology Development) and

Package	Booster	Ta Anvil?	Main Charge	SST membrane thickness	Target
Sliverleaf A					
A1	PBX-9501 (4mm)	yes	PBX-9501 (4mm)	900 μm	1(a)
A2	PBX-9501 (4mm)	yes	TNT (4mm)	900 μm	2
A3	N/A	no	PBX-9501 (4mm)	900 μm	1(a)
Silverleaf B					
B1	PBX-9501 (4mm)	yes	PBX-9501 (4mm)	381 μm	2
B2	N/A	no	TNT (4mm)	381 μm	0
B3	N/A	no	PBX-9501 (4mm)	381 μm	2
Silverleaf C					
C1	PBX-9501 (4mm)	yes	PBX 2mm/TNT 2mm	381 μm	2
C2	PBX-9501 (4mm)	yes	PBX-9501 (3mm)	381 μm	1(a)
C3	PBX-9501 (4mm)	yes	PBX-9501 (4mm)	381 μm	1(a)
Silverleaf D					
D1	PBX-9501 (4mm)	yes	PBX-9501 (4mm)	381 μm	1(b)
D2	N/A	no	PBX-9501 (4mm)	381 μm	1(b)
D3	PBX-9501 (4mm)	yes	PBX 2mm/TNT 2mm	381 μm	0
Sample Class	Description	kh	h (μm)	p-p ampllitude (μr	wavelengt
0	Polished/Diamond	0	0	XX	XX
1(a)	moderate surface	0.2	3.2	6.4	100
1(b)	moderate surface	0.2	3.2	6.4	100
2	high Surface Roug	0.4	4.8	9.5	150
All samples are cylindrical, with diameter 67.430mm.					
Samples 2 mm thick					
Front Surface (towards HE) machined with 16 micro-inch finish					

Table 1: Silverleaf experimental drive configurations and target surface finishes.

Some engineering allowances were requested to aid manufacturability and assembly operations from what was called out in the XTD design release. These included:

Material Substitution for the HE Housing:

304L stainless steel was substituted for Delrin® to enable higher precision manufacturing as well as to substantially reduce the HE housing wall thickness. A reduction in wall thickness was necessary to fit all four packages into the radiographic field of view.

Membrane Thickness:

Initially, engineering requested that a thicker membrane be used to avoid deflection of the membrane/target assembly when the hex package volume is under vacuum. The stainless steel membrane thickness was increased from the physics requested 0.015" thickness to 0.050" to minimize deflection. This

is discussed in further detail in the section below as the 0.050" design proved to be difficult to manufacture as an integrated component of the lid.

Incorporation of Diagnostics:

It was requested that a maximum number of targets be viewable in both Cygnus lines of sight. The Cygnus lines of sight are oriented 60 degrees apart. The field of view of each radiographic line of sight was specified to be 125 mm on a side. Thus the orientation shown in figure 3 was selected. The black circular regions represent the 56 mm diameter diagnostic regions on each target. The parallel orange/white lines represent the 125 mm wide field of view. The two black circles in close proximity to each other attach to one side of the hex housing, the two more distal to each other are on the opposite side of the hex housing as shown on figure 3.

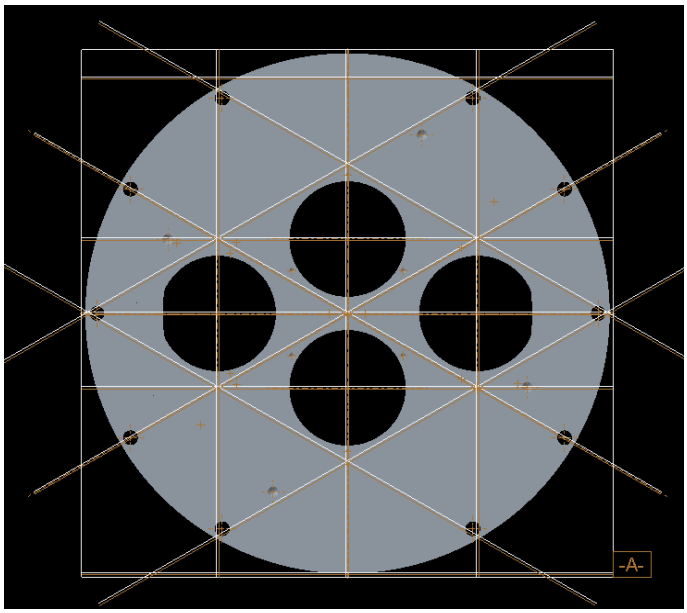

Figure 3: Diagram showing the radiographic lines of sight set 60 degrees apart. The black circles represent target areas to be imaged.

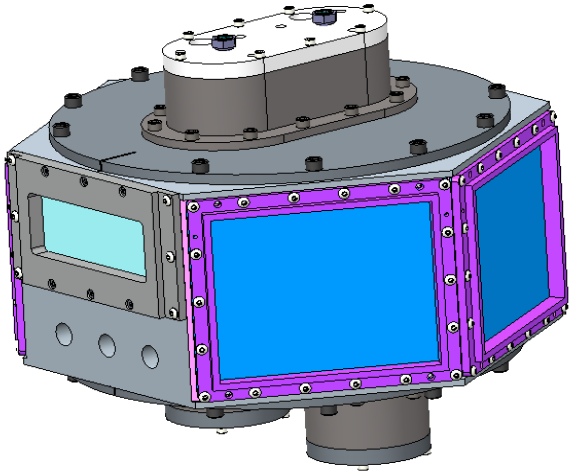

Figure 4: The Hex box housing configuration.

Incorporation of the momentum diagnostics ($LiNbO_3$ pins and Asay foils), as well as PDV, was accomplished utilizing a mounting plate located in the center of the hex housing. Figure 5 shows the desired 35 mm of "free run" from the target surface to the momentum diagnostics. In this configuration, these diagnostics are located within the volume under vacuum. In order to route the diagnostic cables and fibers out of this volume, vacuum feedthroughs were necessary. For Silverleaf, where space was not a limitation, these feedthroughs were commercial items purchased through Conax Technologies. For the Iris and Nightshade experimental configurations, it will be necessary to design a custom, optimized feedthrough to fit within the DPP-2 shipping container and vessel opening size envelopes.

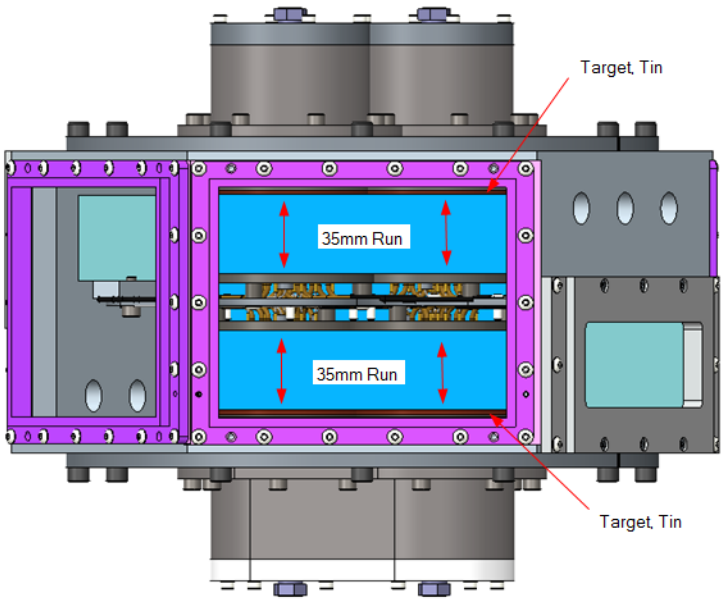

Figure 5: Radiographic view of the package. The diagnostic mounting plate is positioned 35 mm above the targets.

Silverleaf C and D fielded 8 channels each of high explosive burn Time of Arrival Diagnostics (TOAD) located on selected HE drive packages. These diagnostic probes were fielded via penetrations in the stainless steel HE housings.

Engineering Design

Hex Housing Design:

The radiographic lines of sight desired for Silverleaf are similar to what was fielded in a past series of subcritical experiments. The hex housing design for Red Sage is essentially a vertically stretched version of what was fielded in the Bacchus/Barolo series of experiments. The vertical stretch is required to achieve 35 mm of experimental free run and to incorporate a diagnostic mounting plate at the center of the hex housing. This hex housing design fits within the DPP-2 shipping container volume. The use of this shipping container between LANL TA-55 and NNSS DAF will be required for the Nightshade series when nuclear material is present. To demonstrate the feasibility of an acceptable U1a configuration for Nightshade, Silverleaf was limited to these size constraints.

HE Charge Subassembly Design:

There are two different HE charge subassembly types, a wideset one and a narrowset one, which was required to get all four targets into both radiographic lines of sight. These configurations are shown in figure 6. The stainless steel HE housings were populated with HE drive packages as specified by the matrix given by XTD. These subassemblies are then bonded to the stainless steel lid/membrane assembly (using Aralhex®) as part of the last step in the assembly sequence. This bonding operation helps to mitigate membrane deflection when the hex housing internal volume is under vacuum.

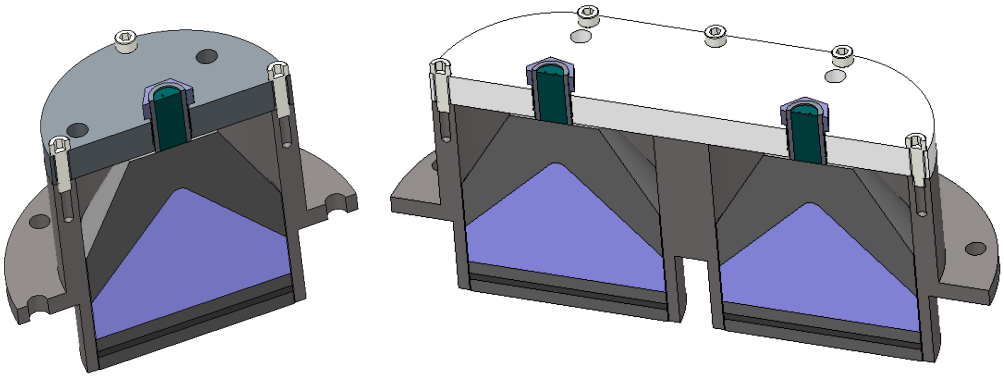

Figure 6: The explosive housing assemblies. On the left is one housing from the wideset design, on the right is the narrowset design.

Stainless Steel Lid/Membrane Assembly Design:

On Silverleaf A, a one-piece design was used with limited success. As mentioned in a previous section, this configuration was difficult to manufacture. When approaching the final thickness of ~0.050", the membrane was very prone to "oil canning" and being punctured by the end mill. Several other methods were attempted to make the membrane/lid out of one piece of material. Ultimately a hybrid plunge electrical discharge machine (EDM) and end milling approach was used for this shot. Although the piece was successfully machined, the resultant membrane was out of specification with respect to flatness.

On Silverleaf B through D, a two piece design was utilized where a 0.015" thick piece of 304L stainless steel sheet stock was laser welded to the larger stainless steel assembly. This process was successful and the membrane flatness remained in spec with respect to the larger stainless steel lid. Additionally, 0.015" was the initial membrane thickness specified in the physics design release.

Final Experimental Configuration:

The Silverleaf series was executed at LANL's Q-Site. The final experimental configuration shown in figure 7 was fielded on a firing table without any relevant size constraints.

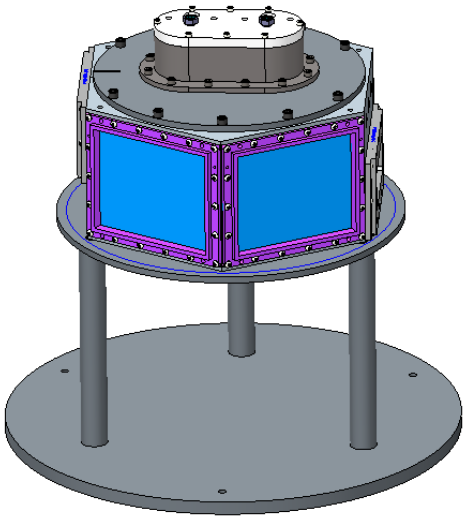

Figure 7: The Silverleaf experimental configuration.

Six experimental drive packages per vessel will be fielded in the Iris and Nightshade experiments of the Red Sage campaign as shown in figure 8. This maximizes the amount of data gathered per vessel shot. While further design maturation is needed, it appears that it will be achievable to install two hex housings in each vessel. The upper hex housing will be in both Cygnus radiographic field of views and will consist of four drive packages similar to the configuration fielded in Silverleaf. The lower hex housing, or another configuration to be determined since this package is not in the radiographic

line of sight, will be mounted underneath the upper hex housing. The notional lower hex housing represents an upper bound on the size constraint and a smaller assembly may be employed for the lower housing.

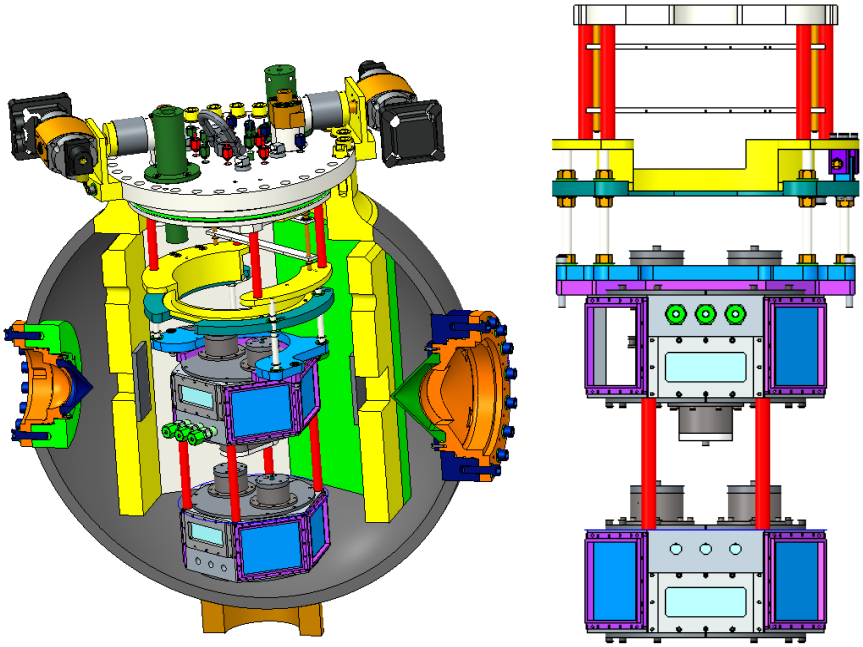

Figure 8: A conceptual model of the Iris and Nightshade vessel configuration with six drive packages. These are incorporated into two hex housing assemblies.

Silverleaf Assembly

Charge Subassemblies:

Stainless steel (SST) HE charge housings were populated with HE and tantalum anvils per physics design requirements. These components were shimmed to be concentric within the stainless steel housing. Each layer of this assembly was bonded to the next using Aralhex® adhesive. A cover was placed onto the back end of the drive package and the detonator cable assembly installed. The remaining volume was back-filled with Nusil® silastic to fill the area behind the plane wave lens portion of the HE drive and to fill any voids between the HE and the stainless steel housing.

The hex housings were populated with diagnostic mounting plates and all PDV probes, $LiNbO_3$ pins, and Asay foils were installed. The cables were routed out of the feedthroughs and sealed.

Targets were bonded to the SST membrane/lid assemblies using Loctite® 496 adhesive. The SST lid/membrane/target assembly was then inverted and the HE subassemblies bonded to the membranes using Aralhex® adhesive. These subassemblies were then attached to the hex housings using machine screws.

Gas Blocking of $LiNbO_3$ Probes:

For Silverleaf A and B, only a moderate vacuum was achieved. On Silverleaf A the best vacuum was achieved was 1.7 Torr with an accompanying rate of rise of 1.4 Torr/min. The lowest vacuum achieved on Silverleaf B was 3.32 Torr with a 4.8 Torr/min rate of rise.

It was suspected that the coaxial momentum pin cables were at fault; thus on Silverleaf C and D, these cables were gas blocked by P-23 personnel. This resulted in an improved vacuum. For Silverleaf C, the lowest vacuum achieved was 186 mTorr with a rate of rise of 32 mTorr/min. For Silverleaf D, 328 mTorr was achieved with a rate of rise of 66 mTorr/min rate of rise. While these pressures were sufficient to make the measurements, the diagnostic target was ≤ 100 mTorr.

CDUs for the Red Sage Series of Dynamic Plutonium Experiments[2]:

Three new solid-state capacitive discharge units, or CDUs (RFD-011 prototypes) were custom built for the Silverleaf series of experiments. Given the complexity of the experiments, it was crucial that the systems deployed are high quality. There are two driving reasons for this. First, the Nightshade experiment will require up to six independently timed detonations. The detonation of each drive package must be timed with sufficient precision to place the ejecta field and spall layer from each target in the correct location for radiographic measurement. Since the drive velocities can vary from target to target, each of the CDUs initiating the packages need to be triggered at different but precise times. Second, the packages to be fielded on Nightshade have tight timing tolerances. The double-shock drive packages are complex, involving shock reflections from both the target and anvil as well as transit shocks through detonated explosive gas products. Given the complexity of the phenomena, precision timing of the initiation train will greatly reduce the uncertainties of the measurement results.

The prototype firing units were built and tested and showed less than 1 ns variability, but these units relied on new and unverified components (direct optically triggered S-38 manufactured by Applied Pulse Power). A decision was made to replace this switch technology with a solid-state technology that has longer demonstrated operation (electrically triggered S-38 manufactured by Applied Pulse Power). The electrical trigger switches resulted in a CDU firing variability of approximately 5 ns. Further testing and verification of the optically triggered technology will continue, with the goal of fielding this technology on the Nightshade experiments.

The cumulative results of CDU variability for Silverleaf experiments A, B, C & D demonstrated about 4 ns standard deviation. The cumulative results of the

[2] This section was contributed by Roger Hall and Gary Liechty (Q-6: Detonator Technology)

CDU/SE-1 detonator bridge wire burst timing variability for Silverleaf experiments A-D was about 7 ns.

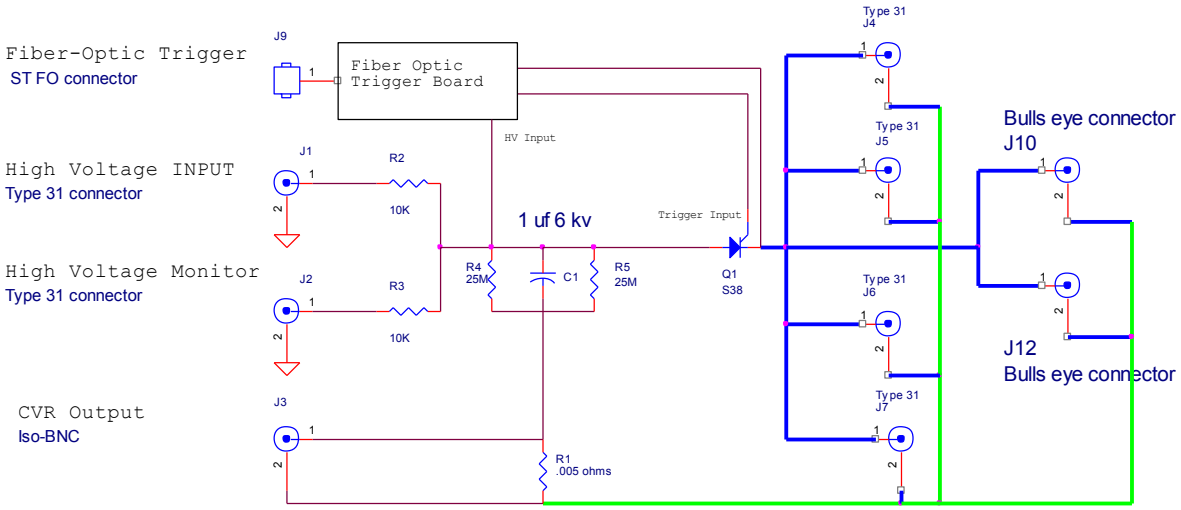

Figure 9. A schematic of the RFD-011 fire set designed for the Silverleaf experiments.

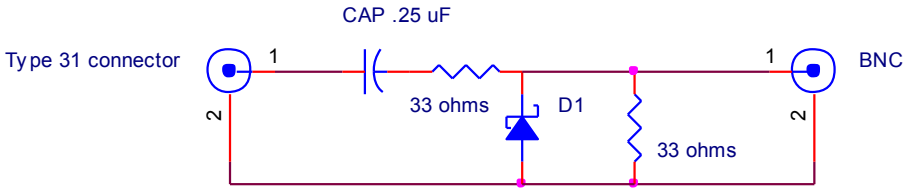

Figure 10: The load-ring indicator circuit.

A load-ring indicator box was attached to the output of the fire-set and provided a well-defined electrical signal indicating discharge output. The load-ring indicator added the ability to accurately time the detonator's bridge wire burst.

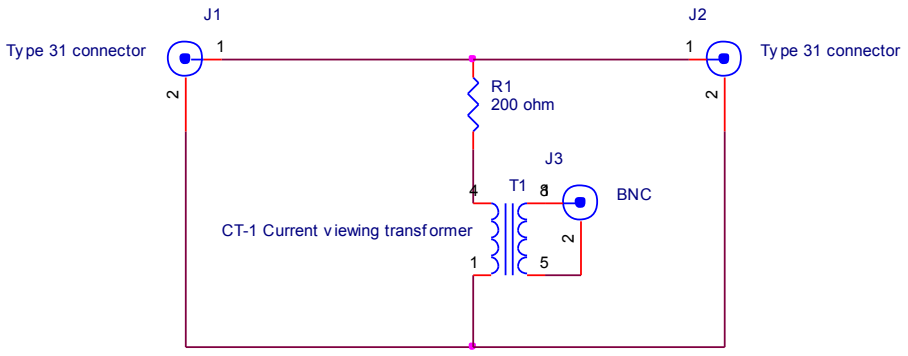

Figure 11: The bridge-wire burst circuit.

Data Systems Fielded and Results

Drive Characterization

Photonic Doppler Velocimetry (PDV)[3]

A variety of PDV systems were fielded on the Silverleaf experiments to maximize the coverage of the drive and shocks in the package. In particular, we fielded:

- a prototype first generation multiplexed PDV (MPDV) system (hereafter "Gen 1"): 32 channels,
- a new third generation MPDV system ("Gen 3"): 16 channels[4], and
- a four point traditional non-multiplexed PDV system ("plain" or "traditional" PDV): 4 channels[5].

The Gen 1 system emits only 10 mW of laser power per channel, so it has a low signal to noise ratio. Since the PDV technique is based on the reflection of light from a surface, this low amount of output power typically reflects off any occluding ejecta, with little light reflecting back from the free surface underneath. In contrast, the Gen 3 system outputs 250 mW per channel so it typically has a much better signal to noise ratio. This also allows measurement of surfaces beneath ejecta clouds and structure within ejecta clouds that are invisible to the Gen 1 MPDV system. However, variation in surface return on the Gen 3 channels indicated that while many channels were able to detect structure within the ejecta clouds, some were not. For this reason, we also fielded four points of traditional PDV. For Silverleaf A, these four PDV points had an output of 600 mW per channel. For Silverleaf B, C, and D, the output laser was increased to give 1.25 W per channel. With this high laser power, detailed structure was observed within the ejecta cloud, of which some was not resolvable using the Gen 3 MPDV system. These differences are shown in figure 12.

In total, 52 channels of PDV were fielded on each Silverleaf experiment – 16 channels of prototype MPDV, 32 channels of Gen 3 MPDV, and four channels of plain PDV. Most of the PDV probes were aimed at the tin targets and the steel lid between the targets. These points were chosen to measure the shock structure and timing of the targets and surrounding materials. In addition, four probes were mounted to the outside of the package to gain a

---

[3] This section was contributed by Pat Harding (P-23: Neutron Science and Technology) and Abel Diaz (National Security Technologies, LLC).

[4] Ed Daykin et. al., "Multiplexed Photonic Doppler Velocimetry for Large Channel Count Experiments", APS Topical Conference on the Shock Compression of Matter 2015, #J3.001.

[5] O. T. Strand, et al., "Compact system for high-speed velocimetry using heterodyne techniques," Rev. Sci. Instr. 77 (2006) 083108-1.

better understanding of how the shocks are transmitted through the hex box walls and feedthroughs. On each target, a probe was located at the center with a ring of three surrounding it. Each of these PDV points was adjacent to a $LiNbO_3$ pin, to provide the drive information necessary to interpret the momentum data. The remaining probes were distributed across the target surface. On Silverleaf C and D, an additional PDV probe with a larger diameter and was added and used with one of the Gen 3 channels which included ranging. The goal of this probe was to improve the sensitivity of the ranging and Gen 3 signals, but the data did not indicate a clear benefit.

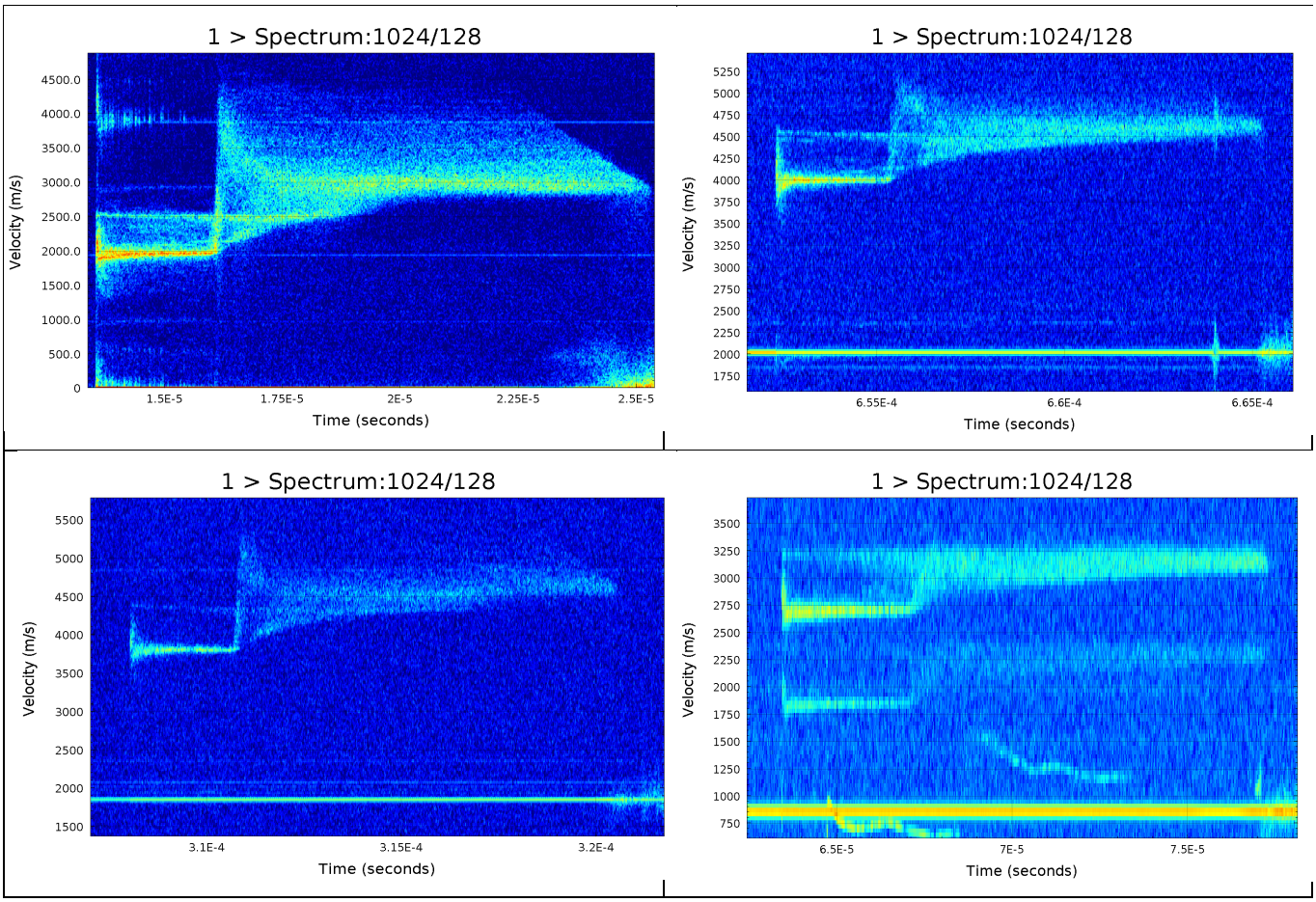

Figure 12: A comparison of the different PDV systems used on Silverleaf. Top left: plain PDV. Top right: Gen 3 MPDV. Lower left: weak Gen 3 MPDV. Lower right: Gen 1 MPDV.

Figure 12 shows a comparison of the various channels. All of these data are from Silverleaf C, target 3. The upper left shows a plain PDV system with 1.25 W per channel. Many detailed structures are seen within the ejecta after second shock. The upper right shows a strong Gen 3 channel. This shows most of the same features are seen as in the plain PDV spectrogram, but they are less distinct. The lower left is another Gen 3 channel with a weaker return signal. While the same general features are seen, it would be difficult to identify them from artifacts without comparison to the higher resolution probes. In the lower right is Gen 1 data. While the general shape of the

ejecta cloud is observable, its features are too weak to observe. Also note that because the prototype system is multiplexed in frequency, signals from other probes can bleed into the field of view.

PDV Features of the Targets:

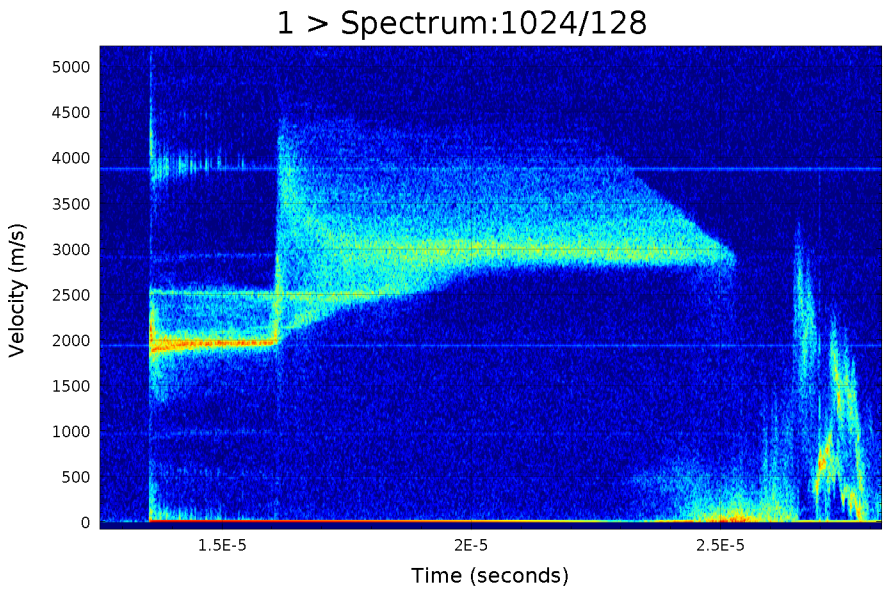

Figure 13: The spectrogram for Silverleaf C3, probe 4.

Although the surfaces and drives were different for each shot, the velocity features seen in the spectrograms were very consistent. For a qualitative analysis of these features, we will refer to figure 13, which is from probe 4 of Silverleaf C, and obtained with a high-power traditional PDV system. Similar features were seen in most channels.

The first shock at the target was seen on all PDV channels. For each target, the timing of the first shock arrivals was within 100 ns of each other from one edge of the target to the other. In addition the three targets all showed first motion within ~300 ns of each other, regardless of the height and composition of the explosive drives indicating that the timing of each detonator was well-chosen. The first shock was seen between 12.3 and 12.6 μs after load ring (timing fiducial) for all PDV points.

After the first shock, the data generally show a well-resolved surface at a near-constant velocity. In figure 13, this surface is seen near 2 km/s. The exception to this was on Silverleaf A, where many of the channels had strong ejecta immediately after the first shock that obscured any possible signal from the tin surface. The speed of this free surface was the primary difference between the different drives – stronger drives with more PBX 9501 had higher velocities, and weaker drives with more TNT had slower velocities. These velocities varied from 1.7 km/s to 2.2 km/s.

One surprising feature in the data was the signature of a second free surface on first shock. This can be seen in figure 13 at 2.5 km/s. This second free

surface signal is thought to be due to the production of a jet of material rising above the surface and the corresponding cavitation of the surface[6]. This feature was observed on all targets except those that had polished/diamond turned surfaces.

In all cases where this second surface was seen, the surface was measured 500 – 600 m/s faster than the main free surface. One feature of this second surface is that it was observed to remain intact and to move with near-constant velocity even after second shock. The second surface was later recollected by the primary accelerating free surface. This is consistent with the interpretation that this is a real sheet of material in the package rather than an artifact of the analysis method or a previously unseen behavior.

For all channels on all shots there was the lack of a visible surface after the second shock. The higher-resolution channels showed a large quantity of ejecta with a lot of structure. We first note a lack of visible ejecta at low velocities – in figure 13 there is no ejecta below 2 km/s immediately after the second shock, with this deficit rising to 2.8 km/s at late times. This is consistent with a (unobservable) free surface recollecting the ejecta as the surface accelerates through the ejecta cloud. Assuming that this feature is the free surface, we see consistent velocities to those observed with the x-ray radiography diagnostic.

At late times, the fastest ejecta arrived at the PDV probes. In our highest-resolution channels, this could be observed directly as a deficit of high-velocity ejecta. In figure 13, this deficit is seen after 23 μs. Integrating the velocities of these ejecta to get a distance traveled, we found the distance traveled matches the distance to the probe (roughly 32 mm), as we would expect.

The second shocks were seen between 2 and 2.5 μs after the first shock on all shots. Because of inhomogeneity in the second shock drive, variation in the timing of the second shock was much larger than for the first shock. The variation was as much as 100 ns.

PDV Features of the Lid (Between Targets):

In addition to the PDV probes aimed at the tin targets, a set of five probes were aimed at the steel lid between the targets. The purpose of these points was to verify that neighboring drive packages did not interfere with one another. Although the spectrogram traces for these points were complicated, the time of first motion was consistent with expectation – coming slightly after the first motion of the points on the nearby targets. The data from the regions surrounding the lone drive package is very similar to the data surrounding the narrowset drive pair, indicating no drive interference.

---

[6] William Buttler et al., "Unstable Richtmyer-Meshkov growth of solid and liquid metals in vacuum," J. Fluid Mech., vol. 703, pg 60 (2012)

Features Seen on External Case Points:

One concern for the Silverleaf design was whether the shock in the walls of the package would damage the data feedthroughs before the end of the experiment; prematurely ending the measurements. To observe this shockwave, we placed four probes on the outside of the hex box at four locations: one on the steel case surrounding the lens, one in the location of the feedthroughs, and two at wall locations in between. On Silverleaf A and B, all four probes were perpendicular to the surface. On Silverleaf C and D, probes 1 and 3 were tilted at a 45-degree angle with respect to the surface. These data indicated that there was no appreciable motion along the direction of the surface. The speeds of the housing surface motion were relatively slow compared to target speeds.

The time of first motion for the probe at the feedthrough was roughly 27 μs after load ring. This is more than a microsecond after the end of trace time, so it does not affect the data. Interestingly, this time corresponds to the vertical line in figure 14 at 28 μs, and is similarly visible in most channels,

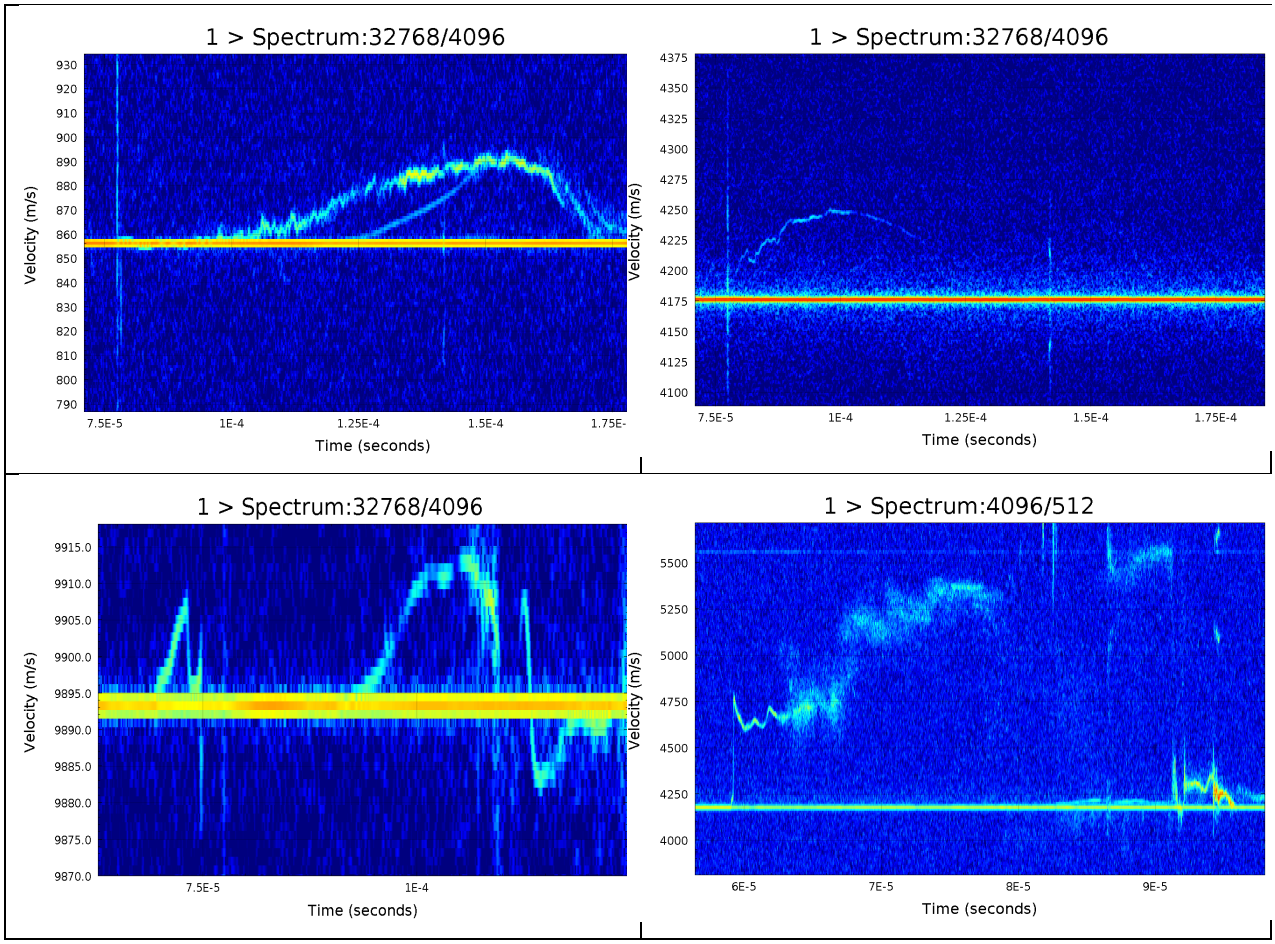

Figure 14: The spectrograms for external case probes 1 (upper left), 2 (upper right), 3 (lower left), and 4 (lower right) from Silverleaf C.

which is after the end of trace. As discussed above, the integrated velocity analysis agrees that we were able to observe the surface (and ejecta) until it arrived at the probe location for all our channels.

Conclusions Based on PDV Data:

The Silverleaf PDV measurements showed many interesting features, including multiple surfaces and significant ejecta. The data shows no early interference between drives, and the data feedthroughs are not disrupted until after the experiments end. In addition, we were able to exercise the PDV diagnostic in a configuration similar to that for Nightshade. Having performed this series, design modifications will be made to better meet the needs of the project.

Broadband Laser Ranging[7]

Broadband laser ranging (BLR) is a new diagnostic and still under development. This is a technique that uses ultra-short pulsed lasers to measure the true distance to a surface along a line of sight[8]. This is especially important for Nightshade, where the ejecta momentum diagnostics require a precise measurement of both the time and position (when and where) of the second shock breakout. While PDV is best for measuring the time of second shock breakout, it is susceptible to signal dropouts. In addition, BLR *directly* measures position, while PDV *assumes* perfect longitudinal flow and then integrates the velocity. The advantage of ranging is this lack of ambiguity.

For Silverleaf, we fielded BLR along the same line of sight as PDV with the use of add/drop filters. This setup worked well, and we demonstrated that the combination of PDV and BLR along the same line of sight gives a temporally and spatially precise measurement of the second shock.

Diagnostic Setup:

The BLR diagnostic is still in a developmental phase and the Silverleaf experiments provided an opportunity to learn how to field it. The details of the diagnostic setup changed for every shot: we explored different lasers, amounts of pre-chirp for the laser pulse, booster EDFA settings, backend optical amplifiers settings, photo detectors, and oscilloscopes. For Silverleaf A, we fielded both a LANL built system and an NSTec built system. A full description of our developmental efforts would be too exhaustive for this report. Instead, we will limit our discussion to a description of the fundamentals of BLR and the general layout of the LANL and NSTec systems.

In figure 15, we show a basic BLR system. A mode-locked laser injects a short (<< 1 ns) pulse of broadband (~20 nm) light into port 1 of an optical

[7] This section was contributed by Patrick Younk (P-23: Neutron Science and Technology).

[8] Brandon Lalone et. al., "Simultaneous broadband laser ranging and photonic Doppler velocimetry for dynamic compression experiments", Rev. Sci. Instrum. 86, 023112 (2015).

circulator. From there, the pulse exits port 2 and enters a Michelson interferometer. One leg directs the light to the surface of interest. The light reflects off this surface and exists the interferometer. The other leg is a reference path with a fiber reflector at the far end. The travel path of the reference leg is constant and is the nearly the same length as the object leg. The object and reference legs are collocated except for the last few meters: such that temperature effects on the relative path lengths are negligible. After entering port 2 of the optical circulator, the object and reference pulses exit at port 3.

Because the light is mode-locked, there is spectral interference between the light in the difference pulses. The spectral interference is a function of the temporal separation of the two pulse (i.e., the relative length of the object leg). The pulses are optically amplified then directed into a spool of fiber many kilometers long. The spool chromatically disperses the light, so that the spectral interference can be detected in the time domain with a fast photo-detector and oscilloscope.

The working range of a BLR system is the maximum difference between the lengths of the two legs that can be measured. For typical designs, this is designed to be several centimeters. The position resolution is a function of the spectral bandwidth of the laser and is typically in the tens of microns range. The laser repetition rate is also the sample rate, and is tens of megahertz.

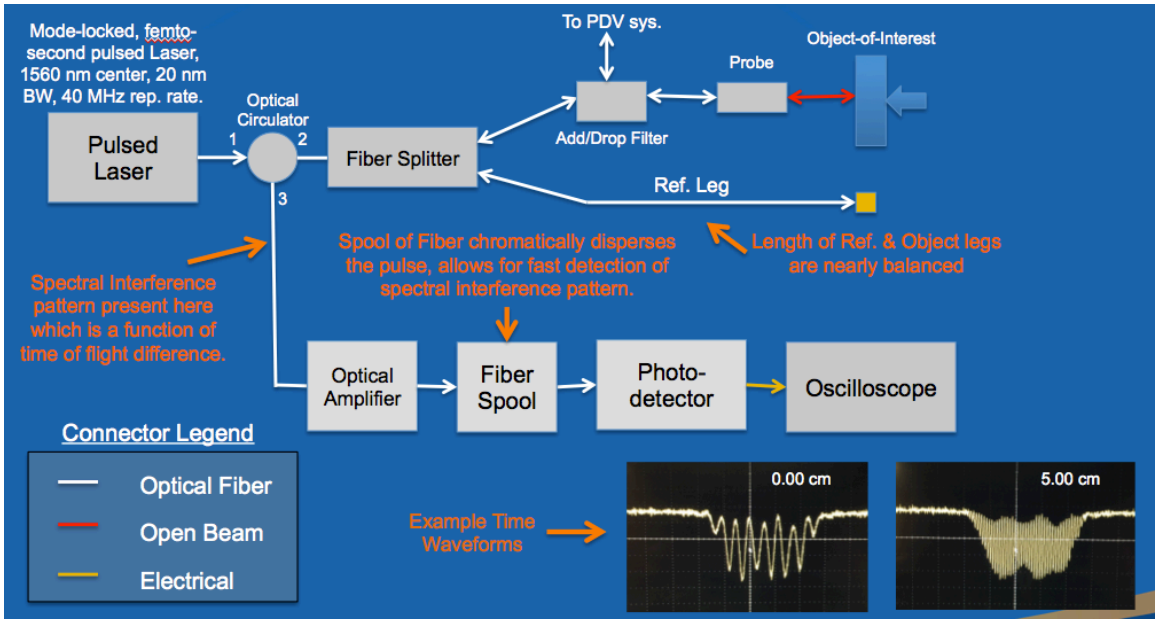

Figure 15: The layout of a basic BLR system. Example waveforms are also shown.

The basic layout that LANL fielded on Silverleaf is shown in figure 15. This system is very similar to the system that is being built for the Eurydice subcritical experiment at U1a, and we believe this design will meet the requirements for the Nightshade series.

The LANL system has several modifications from a basic system. The initial seed pulse in pre-chirped (time broadened) with a 2 km spool to decrease the peak power in the pulse. Pre-chirping allows us to put more energy into each pulse and increase the signal to noise ratio. Pre-chirping also introduces a small amount of Doppler sensitivity (i.e., the position measurement is affected by the speed of the surface). Fortunately, this Doppler sensitivity can be corrected during analysis.

The object leg of the interferometer has an add/drop filter so that PDV light can be directed on to the same fiber to the target. (The add/drop filter shown in the reference leg is not used.) A free-space delay stage allows for the interferometer to be fine-tuned. To economically increase the point count, we duplex points onto a single scope channel. This is performed with a delay spool and a fast optical switch.

The performance specs for the LANL system were:

- Working Range: 60 mm (with zero crossing)
- Position Resolution: 30 microns
- Measure Repetition Rate: 40 MHz

The NSTec system fielded on the first Silverleaf shot was similar to the LANL system. The two main differences were that the pulse was not significantly pre-chirped and that instead of time duplexing two BLR points, the NSTec system duplexed one BLR point and one PDV point.

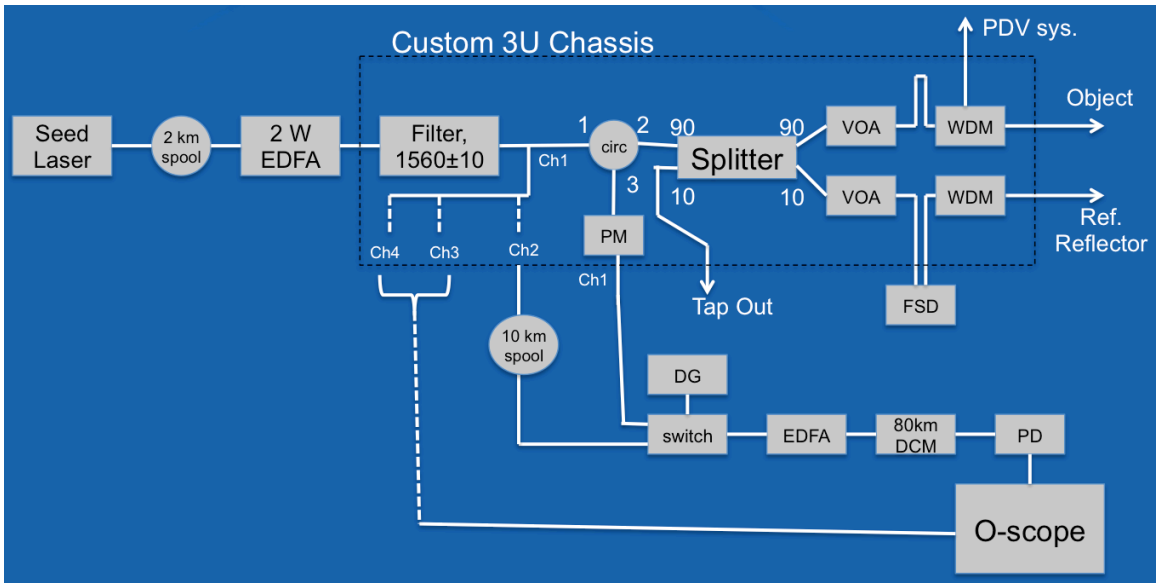

Figure 16: The general BLR setup for the Silverleaf series of shots. The components are – EDFA: Erbium Doped Fiber Amplifier. VOA: Variable Optical Attenuator. WDM: Wavelength Division Multiplexing filter. PM: Power Monitor. DG: Delay Generator. PD: Photodetector.

Conclusions Based on BLR Data:

In figure 17, we show a picture of the LANL BLR diagnostic used on the Silverleaf experiments. Data from Silverleaf B, target 1 is shown in figure 18. For comparison, we show the PDV data recorded on the same line of sight. This data is typical for the Silverleaf series. In the BLR data, the first and second shocks are kinks in the distance vs. time trace. In contrast, shocks are discontinuities in the PDV data.

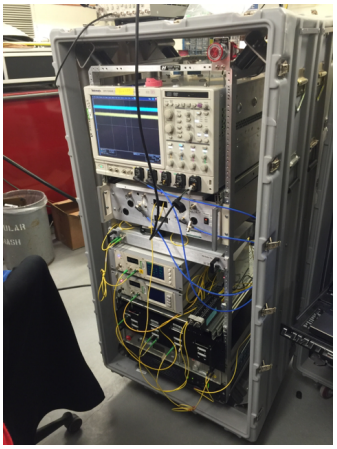

Figure 17: The BLR system used on Silverleaf.

Between first and second shocks, we observe relatively strong signals in both the BLR and PDV data. Also, before second shock the signal has the signature of a single surface (i.e., the energy is not spread over a distribution of positions (BLR) or velocities (PDV). We interpret this to mean we are indeed observing the free surface before and at the moment of the arrival of the second shock. In PDV, the time of second shock is resolved at the 10ns level or better. Through BLR, the position of the second shock is resolved at the 100 micron level or better. Further data analysis can improve the position resolution of the BLR data.

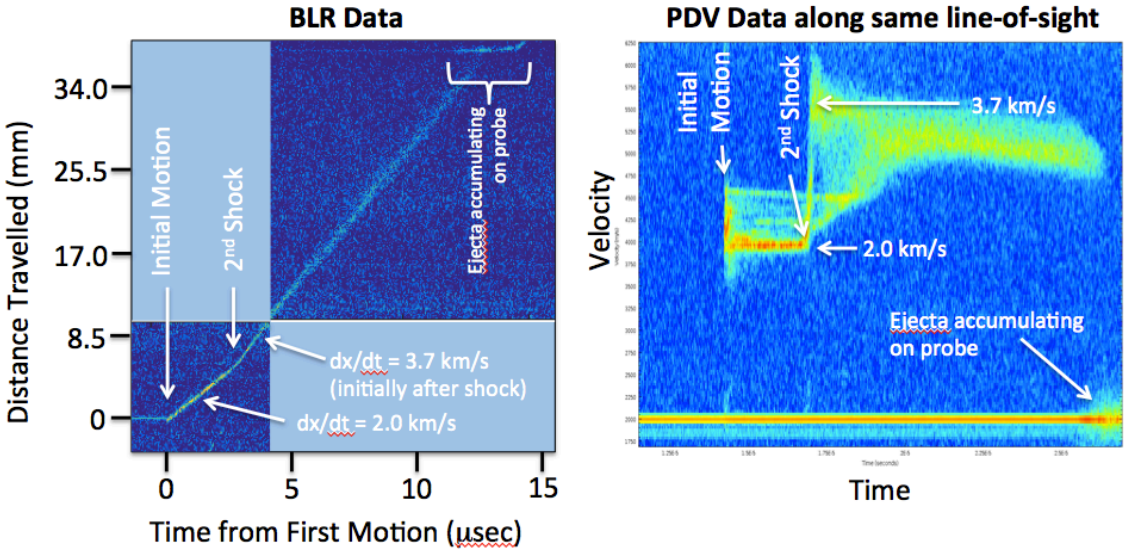

Figure 18: Left: BLR results from Silverleaf B, target 1; Right: Complementary PDV using the same probe.

The velocity calculated from the BLR data (i.e., dx/dt) matches well with what was measured by PDV. This is a constraint on the flow direction relative to the z-axis of the experiment. That is, the flow is indeed mainly longitudinal.

Time of Arrival Diagnostic (TOAD)[9]

Los Alamos continues to develop an optical fiber-based diagnostic to measure explosive burns[10]. Commonly called TOAD, or Time of Arrival Diagnostic, the technique consists of a fiber with a reflective coating placed in contact with the explosive. When the 10 μm core of the fiber is destroyed by the detonation, the reflection of the fiber's end drops. This is recorded by shining laser light down the fiber and measurement with a photodiode.

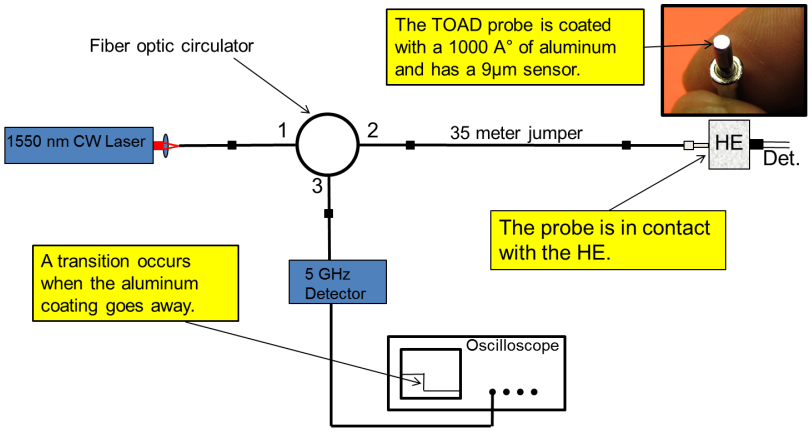

Figure 19: The TOAD measurement system.

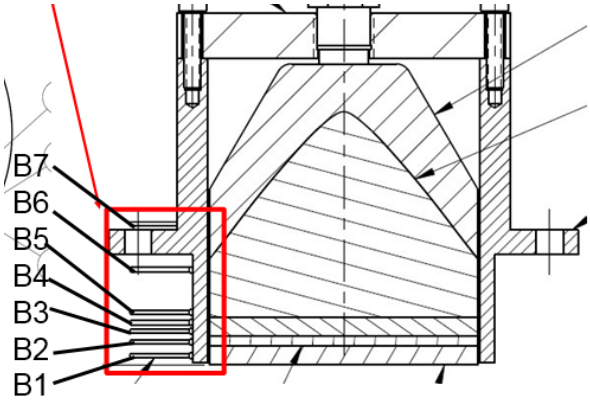

Figure 20: TOAD probe placement on Silverleaf C3. Emphasis was placed on measuring the detonation wave in the last few layers of the drive.

On Silverleaf C and D, holes were drilled into the drive case so that TOAD probes could be inserted in contact with the explosives. These probes were placed at locations that would be valuable in assessing the detonation

[9] This section was contributed by Michael Shinas (J-4: DARHT Experiments and Diagnostics).

[10] Michael Shinas et. al., "Fiber Optic TOAD (Time of Arrival Diagnostic) shock break out validation using PDV", LA-UR-14-24518.

symmetry, speeds and timing. The system returned good data for both Silverleaf C and D, and will prove useful in characterizing the explosive drive for model validation. Figure 21 is a comparison of the burn data for Silverleaf packages C1 and C2. There is a difference in the timing of the detonation wave for the two packages (~50 ns) as it moves through the lens. This is consistent until the detonation reaches the last level before the target, at position 1. There the detonation moves slower through C1, which was a TNT/PBX composite section designed to achieve lower shock pressure.

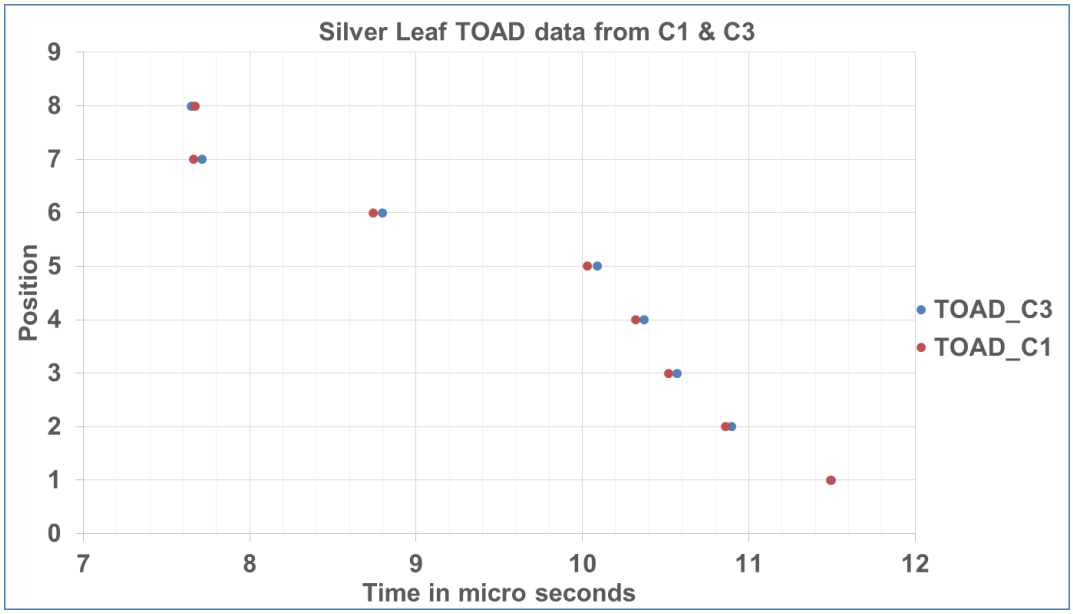

Figure 21: Time of arrival data from Silverleaf C.

Radiography[11]

A soft radiography capability is being developed to support quantitative areal mass density measurements for the Red Sage campaign with the goal of measuring areal mass densities < 0.1 mg/cm^2. For the Silverleaf experiments, a prototype radiography system was fielded. Neither the Marx banks nor the imaging system were optimized for these experiments.

[11] This section was contributed by Danny Sorenson (P-23: Neutron Science and Technology) and Duane Smalley (National Security Technologies, LLC).

Radiographic System Performance:

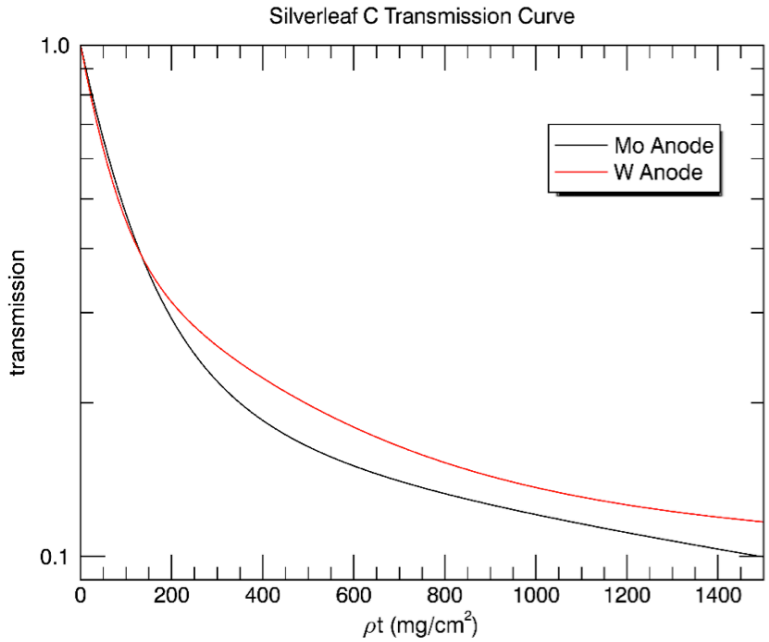

Figure 22: The transmission vs areal density (mg/cm^2) for Silverleaf C. The tungsten vs molybdenum anodes are shown for comparison. Greater contrast separation of closely spaced areal density can be made in regions with large slopes.

The radiography system performed well returning two radiographs for each Silverleaf experiment. The radiographic sources produce a ~50 ns pulse with a dose of about 20 mR at 1 meter. The end point has been estimated to be ~250 keV. A typical transmission versus areal mass curve is shown in figure 22. The curve shows that the tungsten anode provided better density separation for larger areal mass densities. We estimate the sensitivity to be < 1 mg/cm^2. In a previous study[12] using the Super-Saver sources, and a molybdenum anode, sensitivities were estimated to be as low as 0.05 mg/cm^2. For these measurements a thin layer of P43 phosphor was used for the x-ray to light converter.

[12] Michael R. Furlanetto, Report: "Radiographic Options for Red Sage/Nightshade", 3/19/2015, LA-CP-15-00229.

Experiment	Date	Anode (Marx-2)	Anode (Marx -1)	Time (Marx-2)	Time (Marx-1)	Scintillator
Silverleaf-A	7/14/2016	Mo	Mo	18.161	23.149	CsI(Tl)[13]
Silverleaf-B	7/27/2016	W	Mo	18.155	23.143	CsI(Tl)
Silverleaf-C	8/10/2016	W	Mo	18.000	23.000	CsI(Tl)
Silverleaf-D	8/19/2016	W	W	17.161	22.145	CsI(Tl)

Table 2: The x-ray source configuration for the four experiments.

The complete radiography system as it was setup for the Silverleaf experiments is shown in figure 23. The figure indicates the location of the two x-ray source points. The x-ray conjugates were chosen to represent a geometry that can be implemented on the three-foot vessel at the U1a facility. The distance from the x-ray anode/cathode to the center of the physics package was 78.8 cm, and the distance from the center of the package to the scintillator was 16.6 cm. The optical relay system is also shown and was composed of a 4" doublet, a 6" singlet and an 85 mm lens coupled to the framing camera. The lens system relayed a 163 mm diameter circular field of view with a demagnification of eight onto the front end of a three-frame CMOS framing camera.

Not shown in the figure is a prototype pressure and fragment barrier that was bolted onto the front flange of the x-ray port. This protection system was made of 0.25" of Lexan, 0.25" Spectra, and 0.188" of Lexan on the upstream side of the package, and 0.188" of Lexan on the downstream side of the package. This protection held up through all four Silverleaf experiments. The scintillator used for the x-ray to light converter was a micro-columnar CsI(Tl) screen obtained from the company RMD. The CsI(Tl) thickness varied from 500 to 700 μm with a 2 mm graphite backing upstream of the imaging side. The CsI(Tl) was backed with a reflective backing to improve image brightness. This reflective backing increases the light output by a factor of 1.8 but degrades the position resolution due to optical blur. The primary decay time of the scintillators was found to be ~700 ns with a secondary decay time of ~2 μs that accounts for 5% of the total light decay. The secondary decay led to a "ghost" image in the second x-ray pulse image, so that a slight exposure from the first shot could be observed in the second shot. This was removed in processing with a simple subtraction of a scaled early time image from the late time image. The scaling factor of the early time image varied slightly between each shot but was found to be around 10%.

[13] Scintillator thickness was 600 microns for Silverleaf A and B and 700 microns for C and D.

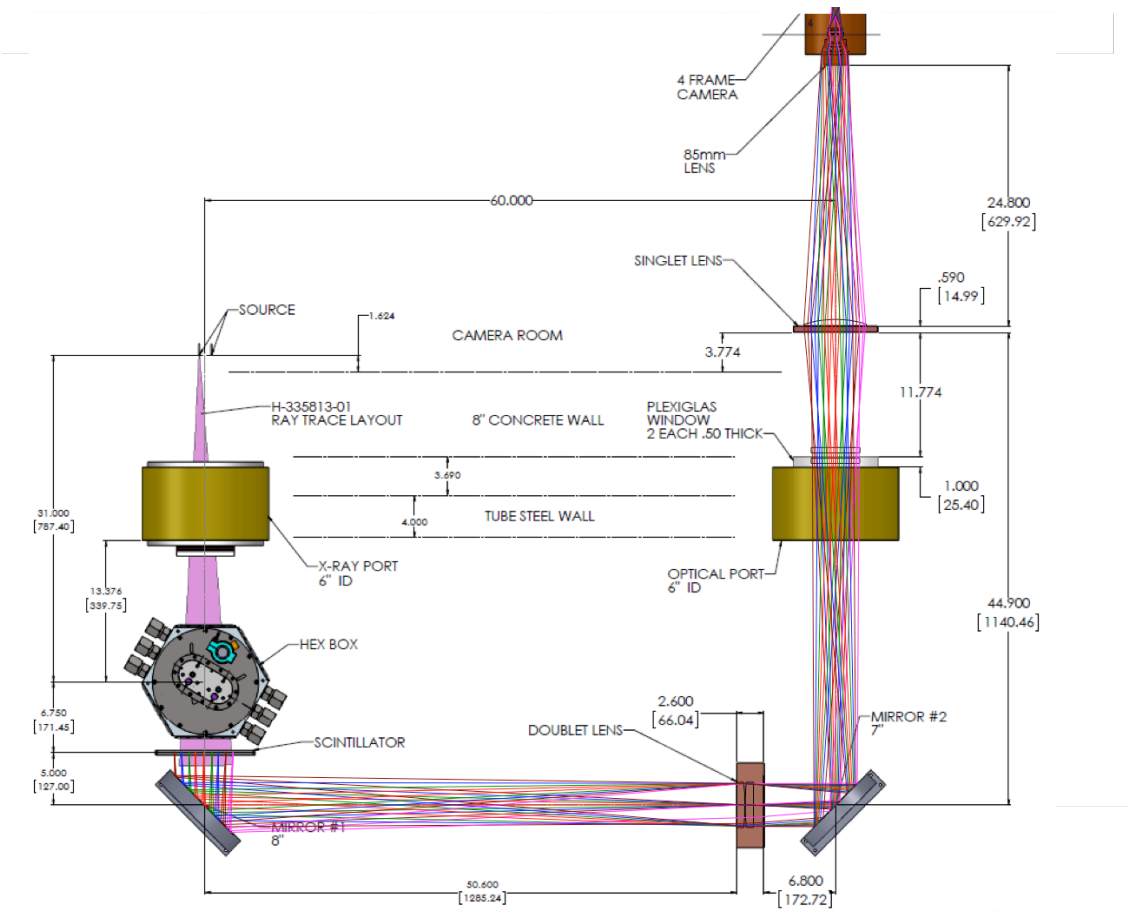

Figure 23: A top view layout of soft radiography system at Q-Site. The 8x optical relay system is shown with the doublet, singlet, and 85 mm lens. The total optical relay system is about 3.4 meters long. X-ray sources and cameras are separated from the shot by the steel as indicated.

Excellent data was obtained for all four Silverleaf experiments. Figure 24 shows an example of the data obtained for the three physics packages in Silverleaf D at the later time. In general, the ejecta field showed roughly cylindrical symmetry. However, there were clearly edge effects observed as seen in the bottom left portion of the image. Figure 25 shows the Abel transformation for package D3 in which ejecta areal densities were obtained.

Conclusions Based on Radiography Data:

Radiography data was obtained on all four Silverleaf experiments. Due to schedule constraints, compromises were made both with the x-ray sources and imaging system. The Super-Saver x-ray sources are being built now, and are expected to provide twice the dose as those used for the Silverleaf experiments. Furthermore, a newly designed optical imaging system will use a much faster scintillator and an optical relay system with more light collection.

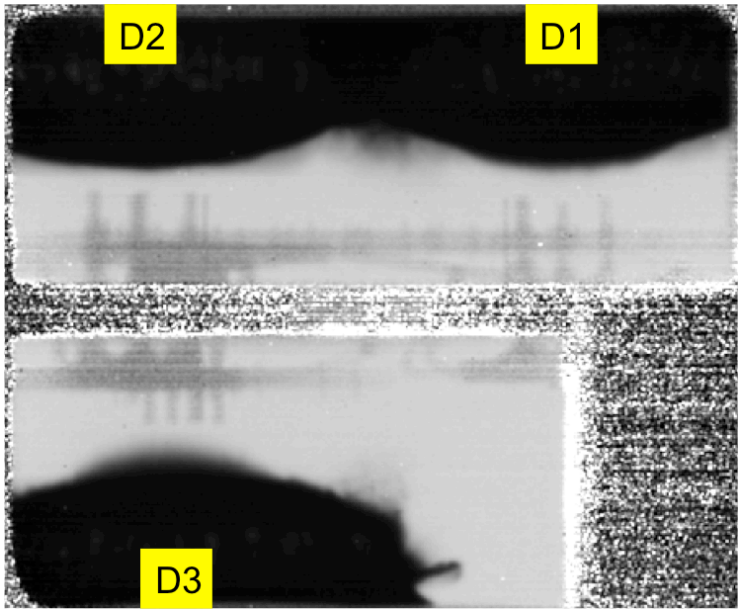

Figure 24: Late time radiography (ratio of raw data to the static) of the three physics packages for the Silverleaf D experiment. Ejecta can clearly be seen for the D3 package at the bottom left of the image. Edge jetting is observed in the image, but appears to be outside the ejecta region.

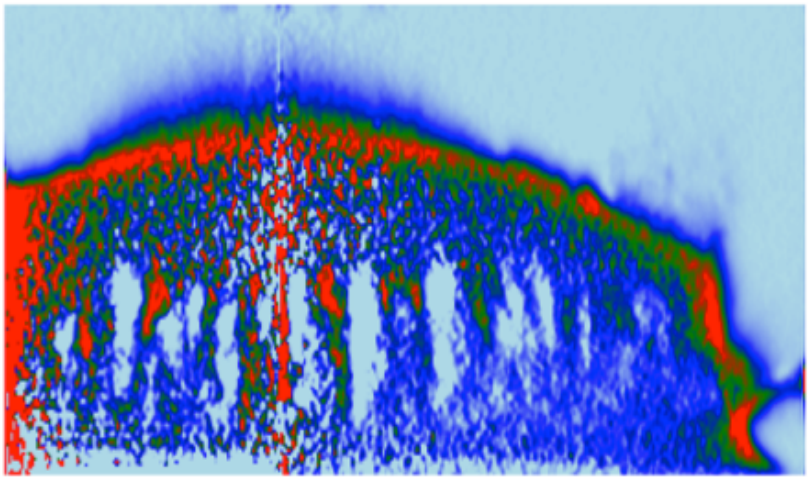

Figure 25: Abel inversion of the package D3 shown in figure 23. Ejecta mass densities are easily extracted from the data.

Momentum Diagnostics

Lithium Niobate ($LiNbO_3$) Pins:

Diagnostic Method:

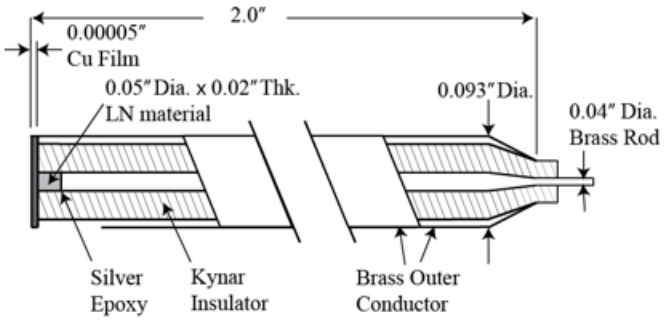

Figure 26: Diagram of the Dynasen piezoelectric probe used on Silverleaf.

Piezo-electric pins using lithium niobate ($LiNbO_3$) crystals was one of the momentum diagnostics fielded on Silverleaf. These pins have been used extensively at Los Alamos National Laboratory for ejecta characterization[14]. The pins provide a voltage proportional to the time derivative of the force applied to them, or

$$V \propto \frac{dF}{dt} = \frac{d^2P}{dt^2}$$

By integrating the pin signal, the momentum transferred to the active area is recorded as a function of time.

One can apply the assumption that ejecta emission occurs nearly instantaneously, and at a known distance from the pin. The time and position of this is measured through drive diagnostics like PDV. This gives the velocity of the cloud impacting the pin as a function of time, from which the mass density of the cloud can be reconstructed.

On Silverleaf, the pins were mounted at a distance of 30 mm from the surface. This distance was a compromise to give radiography as much free field of view as possible, while still keeping the pins relatively close to the initial surface location. Four were mounted above the center of each target, for a total of 12 pins per experiment.

[14] Vogan et. al., "Piezoelectric characterization of ejecta from shocked tin surfaces," J. Appl. Phys. 98, 113508 (2005)

Silverleaf Data Return:

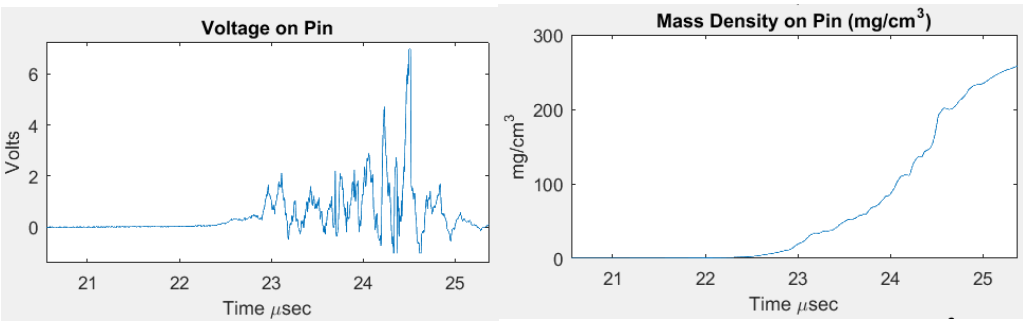

Figure 27: Left: Example signal from a piezoelectric probe. Right: Mass density reconstructed from this signal.

Figure 27 is an example of the data returned from the last experiment, D3. The signal is consistent with typical results in previous work. From the data trace, pin failure appears to occur at around 24.5 μs as the crystal is overloaded by material.

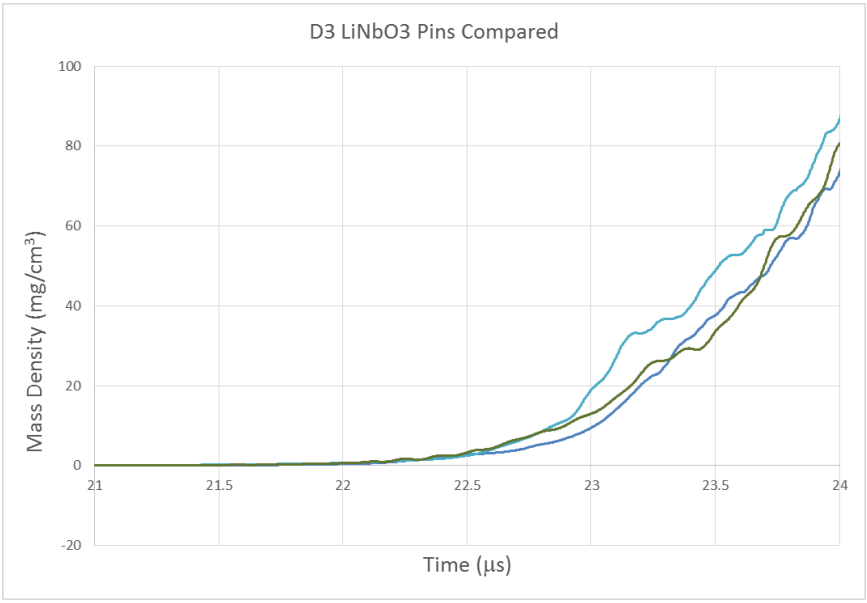

Figure 26: Mass Density reconstructed from three pins on target D3. The signal with the fastest rise was positioned at the center of the package. The others are offset by 7.6 mm.

Figure 26 shows three pin traces from the D3 package overlaid. While the signals show general agreement, the inhomogeneity of the ejecta cloud is visible, especially after 22.5 μs.

Asay foils[15]

Another commonly used momentum diagnostic is the Asay foil[16]. This diagnostic consists of a thin foil placed in front of the target. As the ejecta field impacts the foil, it accumulates momentum and accelerates. This acceleration is measured using optical methods, typically PDV. This technique measures momentum, so is similar to piezoelectric pins in interpretation. However, it is quite different in measurement technique and systematics, and thus is complementary to pin data.

Fielding:

In collaboration with LANL, LLNL fielded a new design for an Asay foil assembly on the Silverleaf experiments. Two variants of the assembly are shown in figure 28 without PDV probes. A complete assembly consists of three basic parts: the green foil holder, one or more foils and a PDV probe. The assemblies in the front row hold three 2.4 mm diameter foils. Two are 100 μm thick pieces of Ti90/Al6/V4 obtained from Goodfellow Corporation. The third foil is a 250 μm thick piece of the same material. The thicker foil is more massive and thus less responsive than the 100 μm foils, but it is also more robust. The assemblies in the back row hold a single 6 mm-diameter 100 μm thick foil. One of each variant was fielded on every Silverleaf package. The large foils were fielded because of their similarity to historic LLNL designs. Single shock experiments at LLNL's HEAF have shown identical performance from large and small foils. Small foils do not necessarily need to be fielded as triplets (in fact the small foils were specifically sized such that they would be interchangeable with piezoelectric pins when singly fielded), but a triplet assembly had the same footprint as the larger single foil assembly and this was considered beneficial.

[15] This section was contributed by Paul Steele, Steve Compton and Jose Sinibaldi (Lawrence Livermore National Laboratory)

[16] Jim Asay et. al., "Ejection of material from shocked surfaces," Applied Physics Letters 29, 284 (1976).

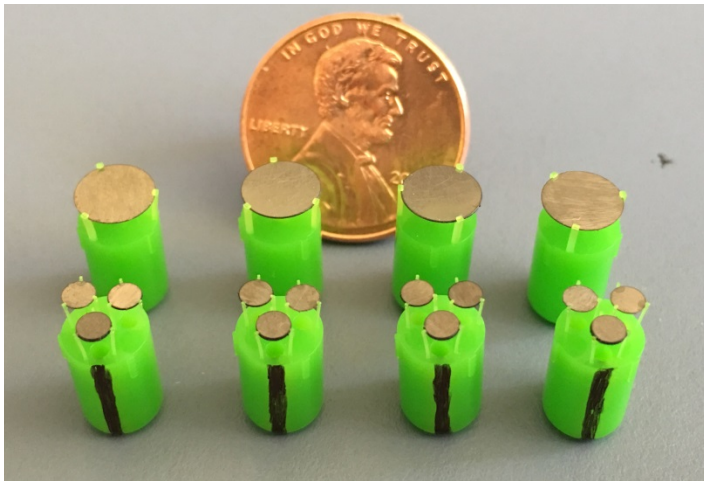

Figure 28: The LLNL Asay foil assemblies.

There were significant assembly issues on at least Silverleaf A and B. The metal foils were placed in the green foil holders after the holders were secured inside the hex package. This greatly limited accessibility and made subsequent assembly difficult. As a result, on Silverleaf A and B many of the small legs supporting the foils were broken. This is not necessarily a problem in and of itself (the legs are intended to break during a real experiment), but the lack of a full complement of legs means that the foils can tilt. Furthermore, excess glue was visible on the foils. This changes the foil mass and thus the sensitivity. Without knowing the foil mass accurately, the data can not be properly analyzed.

For Silverleaf C and D, the Asay assembly procedure was improved. The foils were glued into the foil holders outside of the hex package at LLNL. The LANL team then inserted the preassembled foils and holders into the hex package, glued the holders in place and inserted the PDV probes.

Silverleaf Asay Foil Data:

The most remarkable feature of the Silverleaf Asay foil data was its variability. Figure 29 shows Asay foil data from the D3 target. In a constant ejecta field, the curves for the three 100 μm thick foils should be identical. The curve for the 250 μm foil should have essentially the same shape but merely be proportionally slower. Figure 30 shows Asay data for the Silverleaf C2 target. Once again, three of the curves should theoretically be identical while the fourth proportionately slower.

It is possible that assembly problems were still present, but this is not visible in the assembly photographs for Silverleaf C and D. It is unlikely that tilted foils or excess glue alone can explain all the differences in the data. In fact, it is almost certain that different foils are seeing physical variation in the ejecta field. Radiography, video and PDV data all suggest second-shock variation and non-uniformity on most shots. Interestingly, initial pin analysis on D3 appears to agree fairly well with radiography, and pin variability appeared

less than that of the foils. This could be a statistical fluke, but it may also be indicative of more interesting phenomena.

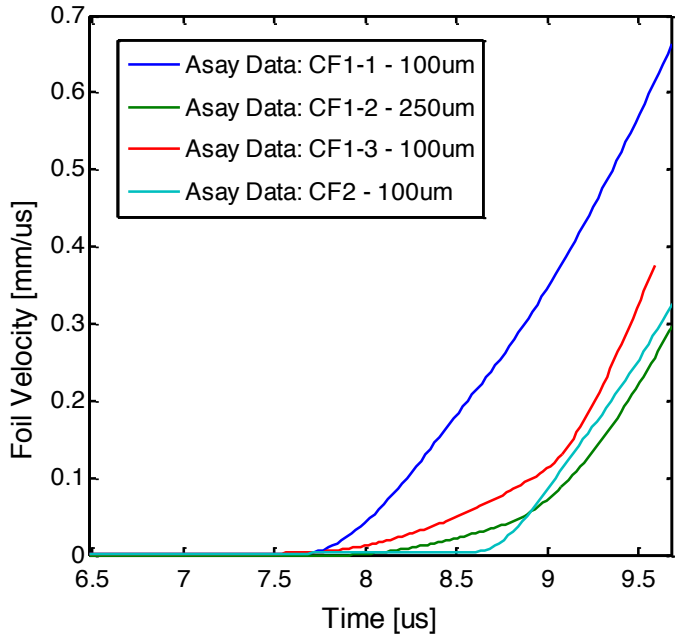

Figure 29: Asay foil data from the Silverleaf D3 target.

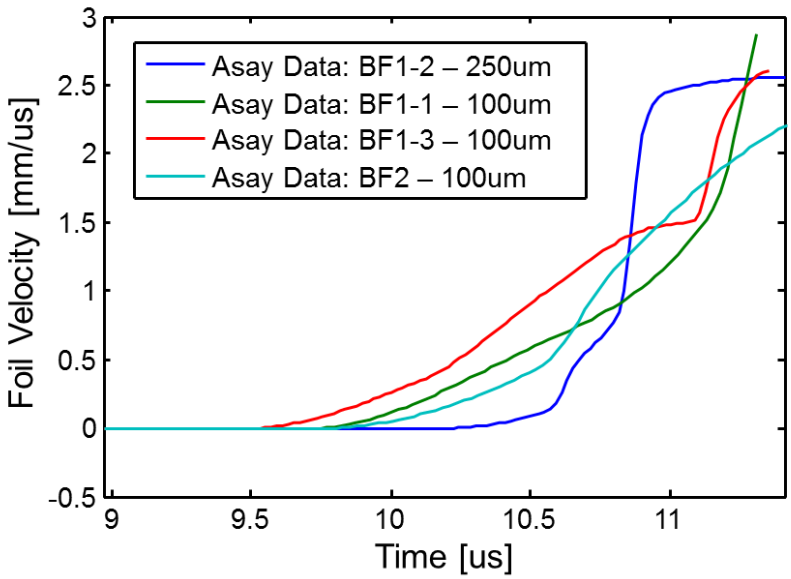

Figure 30: Asay foil data from the Silverleaf C2 target.

The Asay foils probed a much smaller region of the ejecta cloud than did the pins or radiography. The PDV probe used in an Asay foil assembly only directly probed a ~300 μm spot on the foil. Pins have a 0.05" or 1.27 mm diameter crystal with nearly 18 times the area of the PDV probe spot. In processing, radiography integrates (and thus essentially averages) across the entire ejecta cloud. This difference in spatial resolution does not seem to be an issue in single shock experiments, but preliminary modeling suggests that the spall and recollection process introduces physical complexity in the second shock. In particular, there may be "surface mess" with strong density fluctuations on a few hundred micron size scale. This is tantalizingly close to the Asay probe spot size. It is possible that the Asay foils are actually resolving the predicted features. Either way, more investigation on this matter is warranted.

Other Diagnostics

High Speed Optical Imaging

On the Silverleaf experiments, only one window of the hex housing was used for radiography, leaving another window unused. This provided the opportunity to field high-speed imaging on the experiment. We used a Shimadzu camera with a frame rate of 200 ns taking 128 images, and the images were backlit with a magnesium bulb.

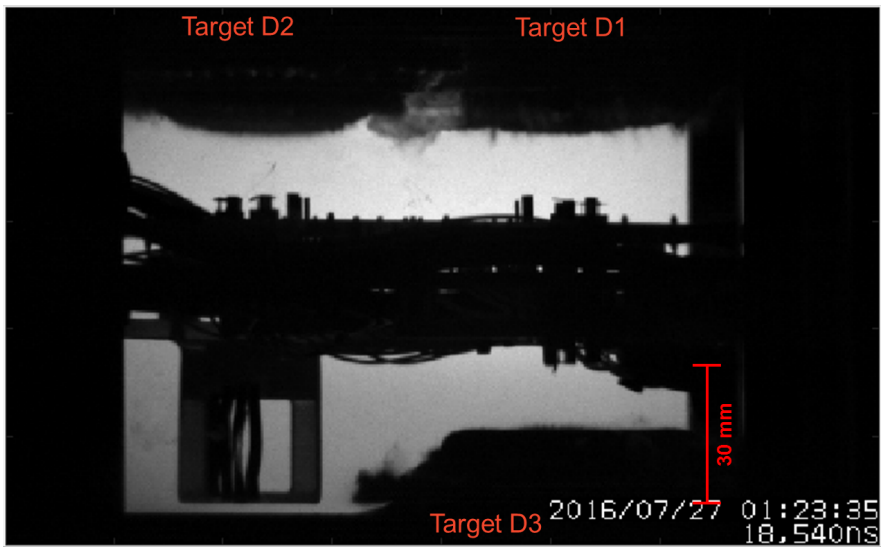

Figure 31: High-speed image of the Silverleaf targets, 5 μs after the surface begins to move.

On Silverleaf A there was a failure in the camera control system and we missed the data. On the three remaining shots, video data was collected.

There are a number of advantages to the high-speed images. First, the frame rate is high enough to see the evolution of the targets. Also, imaging is very sensitive to small amounts of material that are invisible to radiography. The

disadvantage of the imaging is it that it is not quantitative in understanding the character of the ejected clouds.

In general, the images reveal a very smooth planar drive early in the motion, which evolves into an inhomogeneous emission after the second shock arrives at the surface. It also reveals material flying sideways from each package, which can cross to the neighboring field of view. For the most part this material stays behind the free surfaces and outside the diagnostic region, but is an interference that may need to be mitigated in Nightshade design revisions.

Witness Plates[17]

We are very concerned about maintaining the integrity of the vessel during and after the experiment at U1a. The high-explosive load is well within pressure tolerance of the vessel, so the greatest threat will be from fragments impacting against windows and feedthroughs. To develop an understanding of the fragmentation threat, steel witness plates were installed on Silverleaf C and D near the package.

The Silverleaf packages produced fragments that penetrated the plates as shown in figure 32. The 6 mm thick A36 steel witness plate had holes as large as 20 mm x 35 mm located ±150 mm from the center of the plate. The witness plate was used to qualitatively establish the energy and trajectory of the fragments that would impact the internal structures of the Nightshade vessel.

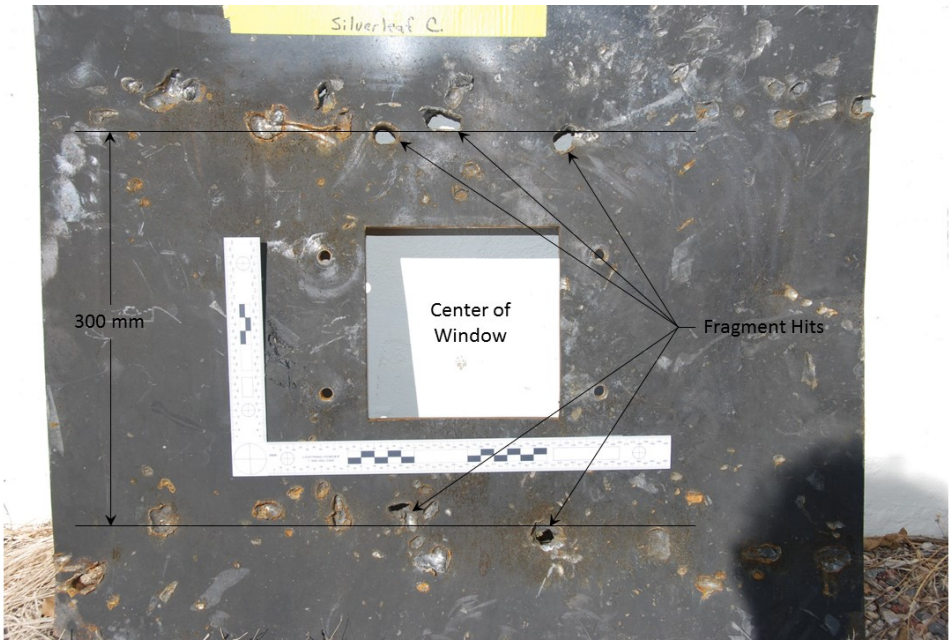

Figure 32: The witness plate from Silverleaf C. The x-ray port was set in the center of the plate.

[17] This section was contributed by Robert Gentzlinger (A-3: Technology Applications).

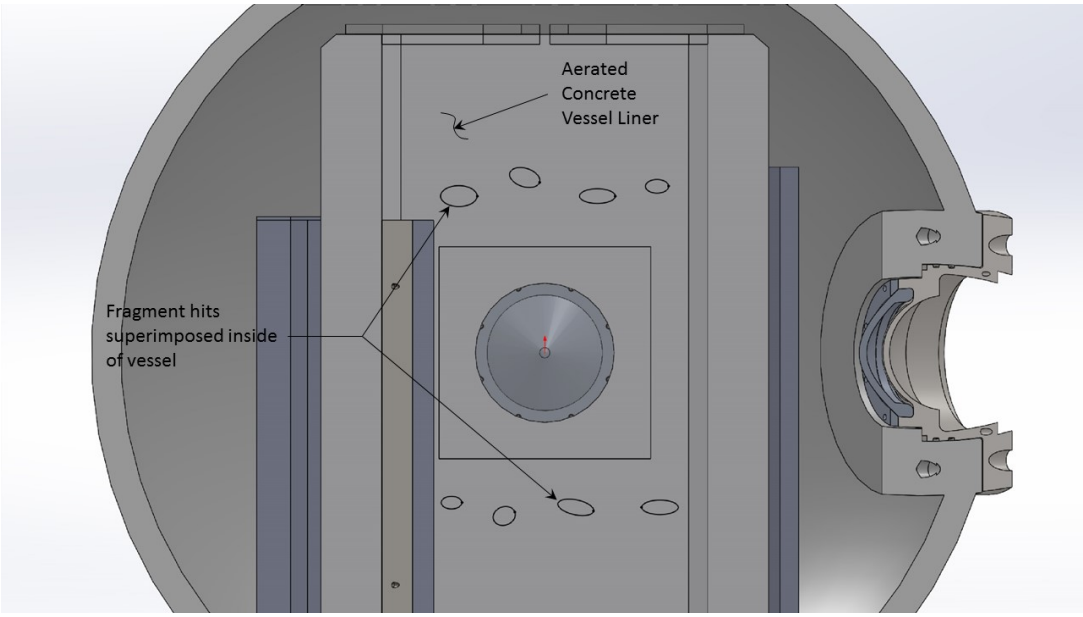

Figure 33: The Silverleaf fragment pattern superimposed on the U1a internal vessel structure.

Figure 33 shows where the fragments would strike the internal vessel structures. A window designed to allow soft x-rays to reach the test assembly may not be able to withstand the impact of these fragments. However, the fragments impacted far enough above and below the window that it would not have been breached.

Diagnostic Comparisons

Drive and Signal Timing

We have begun an analysis comparing the various diagnostic returns. In general, the Silverleaf C and D packages returned the best quality data, as we had implemented a number of improvements to the manufacturing and build of the packages. For our comparisons, we focus on these experiments.

Figure 34 shows an examination of the signal start and end times for the various diagnostics on Silverleaf D3. Combined in this figure is the surface motion estimates from PDV and radiography, as well as PDV estimates of the ejecta cloud motion. The height and signal times for the momentum diagnostics have been added as well. The overlay shows consistency among the various diagnostics, even with variation stemming from the inhomogeneity of the ejecta cloud.

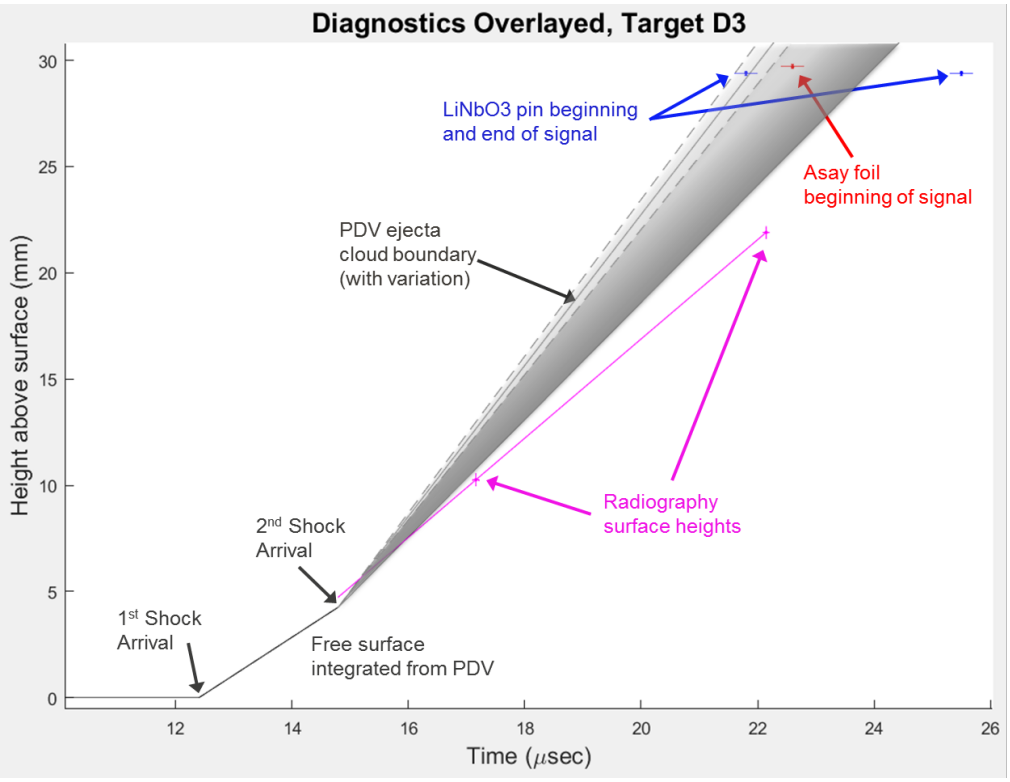

Figure 34: The Silverleaf diagnostics overlaid in time and location. In this figure we have combined: (gray) Integrated PDV data for the surface and ejecta cloud; (magenta) Radiography surface heights; (blue) Piezo-electric pin start and end times; and (red) Asay foil beginning of signal.

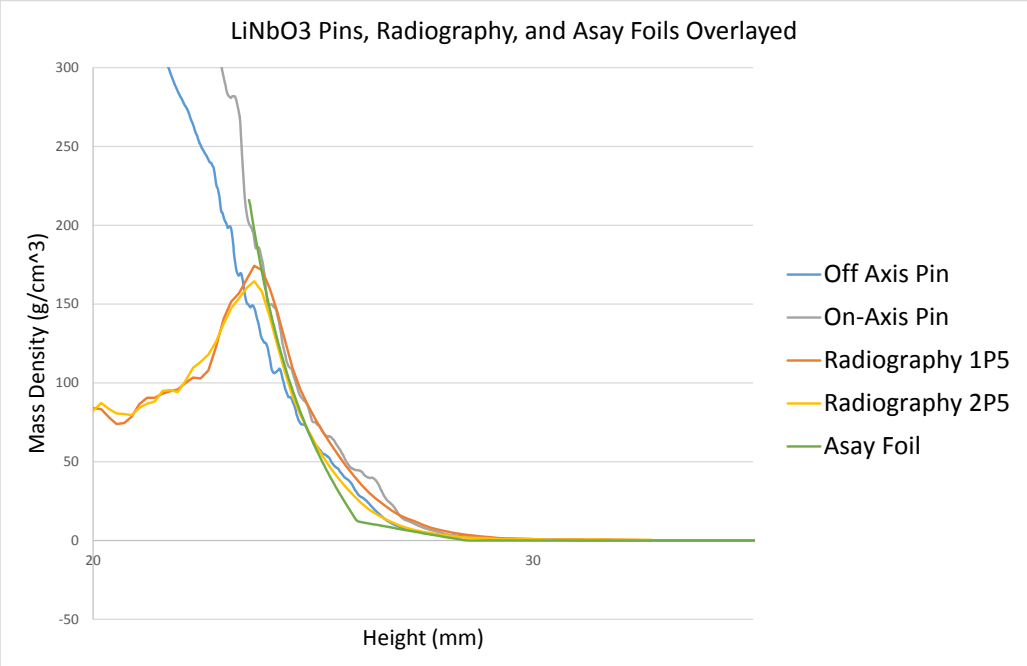

Figure 35: A comparison of the ejecta diagnostics. A time shift has been applied between diagnostics.

Ejecta Diagnostics

Figure 35 shows an overlay of the various ejecta diagnostics. Specifically, the momentum diagnostics have been transformed from density as a function of time to density as a function of space at the second radiograph time. There is a caveat to this figure, which is that an arbitrary shift has been applied to the relative diagnostic heights. At the time of this report, we are still chasing down the source of this discrepancy, but find it promising that the shapes and values of the curves show agreement within the apparent variability of the emission.

Drive Interference

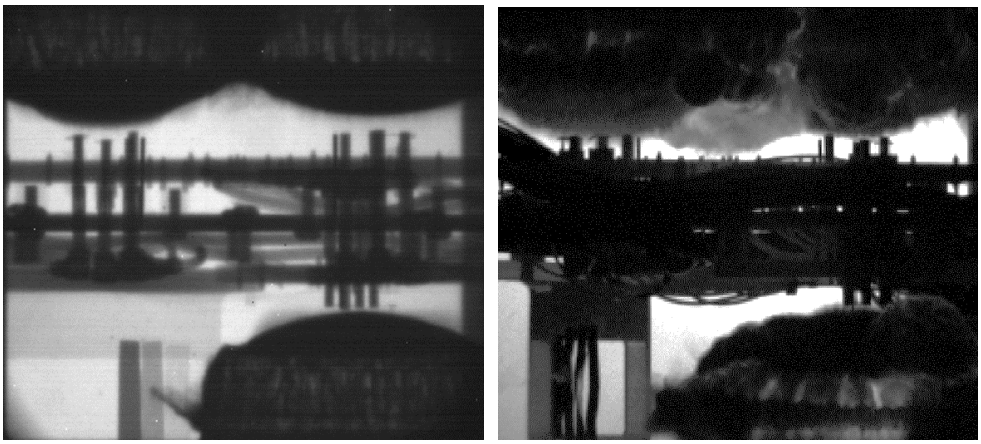

Figure 36: Images of the Silverleaf B experiment, both 23 μs after load ring. On the left is the radiographic image, on the right is optical video.

Figure 36 is a radiograph of Silverleaf B at 23 μs next to a frame from the high-speed optical imaging at the same time. The optical image is far more sensitive to HE gasses as well as slight amounts of material. In both images, there is clear jetting from the edges of the targets. This jetting does not appear to enter the diagnostic region of the neighboring package, nor interfere significantly with its behavior. The most cross-drive interference results from the gasses jetting between the packages, as seen at the top of the images. For the most part this does not interfere with the data integrity, but it is still a point of concern for the future experiments, and will we will consider methods to mitigate it. Drive interference between radiographic fields of view is minimal. This conclusion is supported by velocimetry measurements, which show no drive interaction through arrival of the second shock.

Summary and Conclusions

The Silverleaf experiments were a successful exercise of the prototype Nightshade package to be fielded at the U1a facility in Nevada. The success of this series was the result of the efforts of a large, multi-laboratory team of people from LANL, NSTec, and LLNL.

The Silverleaf package was a good initial design, and succeeded in meeting the constraints for fielding at U1a. In addition, all the diagnostics functioned and returned data, one of the major technical concerns of the Nightshade series. The various ejecta diagnostic agree well with each other. In addition, the series provided a number of benefits to the Nightshade campaign and future SCE work:

- We have seen little drive interference, and have begun examining methods to mitigate the cross-contamination that does exist.
- We used the opportunity to develop an understanding of the fragmentation pattern of the device. This will be valuable in the design of the vessel mitigation.
- While the package design was good, it is not perfect. As a result of this series, we have a number of design improvements to implement for the Nightshade experiments. These improvements cover many aspects of the design, from diagnostic improvements to manufacturing and assembly methods that will result in a more efficient and higher quality experiment.
- We have designed and implemented a new fireset in support of Silverleaf/Nightshade. Not only will this benefit Red Sage, but the opportunity to modernize the design and components of the sets will benefit the entire SCE program.
- This was an opportunity to field improved ranging and PDV systems in advance of the Eurydice series. The experience with these diagnostics has already resulted in improvements to be implemented on current experiments in Nevada.

Acknowledgements

The success of the Silverleaf experiments results from effort from a large and dedicated group of people. These include:

Los Alamos National Laboratory

A-3: Bob Gentzlinger

C-PCS: David Oschwald

J-4: Daniel Creveling, Dean Doty, Steve Gilbertson, Michael Shinas

J-8: Ray Guffee, Daniel Naranjo, Steve Rivera

M-6: Chris Campbell, Angelo Cartelli

MST-7: Derek Schmidt

P-23: Matt Briggs, Billy Buttler, Jeremy Danielson, Dana Duke, Pat Harding, Tymothy Mangan, Ruben Manzanares, Patrick Medina, Pete Pazuchanics, Jeremy Payton, Danny Sorenson, Benjie Stone, Lenny Tabaka, Patrick Younk

PF: Daniel Aragon, Ernie Aragon, Martin Herrera, Vince Hesch, Tony Martinez, Louis Montoya, Jose Olivas

Q-6: Roger Hall, Gary Liechty

Q-7: Rueben Roybal

W-5: Craig Cunico, Robert Gonzales, Rudy Originales, Morgan Tompkins, David Villareal

XTD: Amy Bauer, Mike Furlanetto, Carl Hagelberg

National Security Technologies

STL: Brandon Lalone, Jerry Stevens

LAO: Stuart Baker, Andrew Corridor, Abel Diaz, Al Lopez, Dane Morgan, Dave Phillips, Duane Smalley, Andrew Smith

NLV: Ed Daykin, Mike Hanache, Mike Pena

Lawrence Livermore National Laboratory

Corey Bennett, Steve Compton, Louis Ferranti, Adam Lodes, Jose Sinibaldi, Paul Steele